Discrete somatic niches coordinate proliferation and migration of primordial germ cells via Wnt signaling

Andrea V. Cantú, Svetlana Altshuler-Keylin, and Diana J. Laird

Department of Obstetrics, Gynecology and Reproductive Sciences, Center for Reproductive Sciences, Eli and Edythe Broad Center of Regeneration Medicine and Stem Cell Research, University of California, San Francisco, San Francisco, CA 94043

Inheritance depends on the expansion of a small number of primordial germ cells (PGCs) in the early embryo. Proliferation of mammalian PGCs is concurrent with their movement through changing microenvironments; however, mechanisms coordinating these conflicting processes remain unclear. Here, we find that PGC proliferation varies by location rather than embryonic age. *Ror2* and *Wnt5a* mutants with mislocalized PGCs corroborate the microenvironmental regulation of the cell cycle, except in the hindgut, where *Wnt5a* is highly expressed. Molecular and genetic evidence suggests that *Wnt5a* acts via *Ror2* to suppress *β-catenin*–dependent Wnt signaling in PGCs and limit their proliferation in specific locations, which we validate by overactivating *β-catenin* in PGCs. Our results suggest that the balance between expansion and movement of migratory PGCs is fine-tuned in different niches by the opposing *β-catenin*–dependent and *Ror2*-mediated pathways through *Wnt5a*. This could serve as a selective mechanism to favor early and efficient migrators with clonal dominance in the ensuing germ cell pool while penalizing stragglers.

Introduction

A central question in development is the extent to which cellular decisions are controlled by intrinsic or extrinsic cues. Primordial germ cells (PGCs), the precursors of eggs and sperm, are among the first embryonic lineages established (Laird et al., 2008). The subsequent migration of this small population through the early embryo to the nascent gonads is highly conserved among organisms (Nieuwkoop and Satasurya, 1979, 1981). *Drosophila melanogaster* and zebrafish have provided powerful models for identifying genes and pathways involved in PGC migration (Kunwar et al., 2006), although much less is known in mammals. After specification, mouse PGCs at embryonic day 7.5 (E7.5) migrate from the base of the allantois into the hindgut endoderm. They travel within the expanding hindgut epithelium and into the dorsal mesentery before colonizing the gonadal ridges by E11.5, after which sex-specific differentiation proceeds (Chiquoine, 1954; McLaren, 2003). This migration is asynchronous; those first to exit the hindgut are speculated to be "pioneer" germ cells that arrive first in the gonads and guide additional PGCs to their location (Gomperts et al., 1994).

Distinct from other models, mammalian PGC migration is concurrent with proliferation (Richardson and Lehmann, 2010), raising the question of how cells divide while moving. In mice, the number of PGCs expands from ∼45 at E7.5 to ∼200 at E9.5 (McLaren, 2003; Seki et al., 2007) and ∼2,500 at E11.5 (Laird et al., 2011) and peaks to ∼25,000 at E13.5 (Tam and Snow, 1981). Precise control of the cell cycle is suggested by differential rates of PGC proliferation during their migration (Seki et al., 2007); however, the underlying mechanisms remain unclear. Understanding this dynamic management of proliferation in PGCs could yield insights into the origin of germ cell tumors as well as evolutionary mechanisms that shape the gamete pool.

Several Wnt ligands have been implicated in PGC development: *Wnt3* and *Wnt3a* in specification (Ohinata et al., 2009; Bialecka et al., 2012; Aramaki et al., 2013; Tanaka et al., 2013); *Wnt5a* and its receptor, *Ror2*, in migration (Laird et al., 2011; Chawengsaksophak et al., 2012); and *Wnt4* in female sex differentiation (Vainio et al., 1999; Chassot et al., 2012). Both establishment and sex differentiation of PGCs use the *β-catenin*–dependent, canonical arm of the Wnt pathway (Chassot et al., 2008, 2011; Aramaki et al., 2013), but its function in migratory PGCs is unknown. This well-studied pathway regulates cell fate decisions and proliferation, and recent work suggests that the context of receptors and ligands determines the predominant downstream signaling pathway in an individual cell (van Amerongen and Nusse, 2009; van Amerongen et al., 2012). In this way, Wnts can be broadly used throughout development to simultaneously regulate many cell types and processes.

Here, we find that proliferation of PGCs during development varies according to successive embryonic location rather than by cell-intrinsic mechanisms. We show that distinct niches

Correspondence to Diana J. Laird: diana.laird@ucsf.edu

Abbreviations used in this paper: ChIP, chromatin immunoprecipitation; DE, differentially expressed; E, embryonic day; FDR, false discovery rate; GOF, gain of function; GSEA, gene set enrichment analysis; ISO, isolation; MEF, mouse embryonic fibroblast; n-βcat, nuclear *β-catenin*; PGC, primordial germ cell; WT, wild type.

The Rockefeller University Press $30.00
J. Cell Biol. Vol. 214 No. 2 215–229
www.jcb.org/cgi/doi/10.1083/jcb.201511061

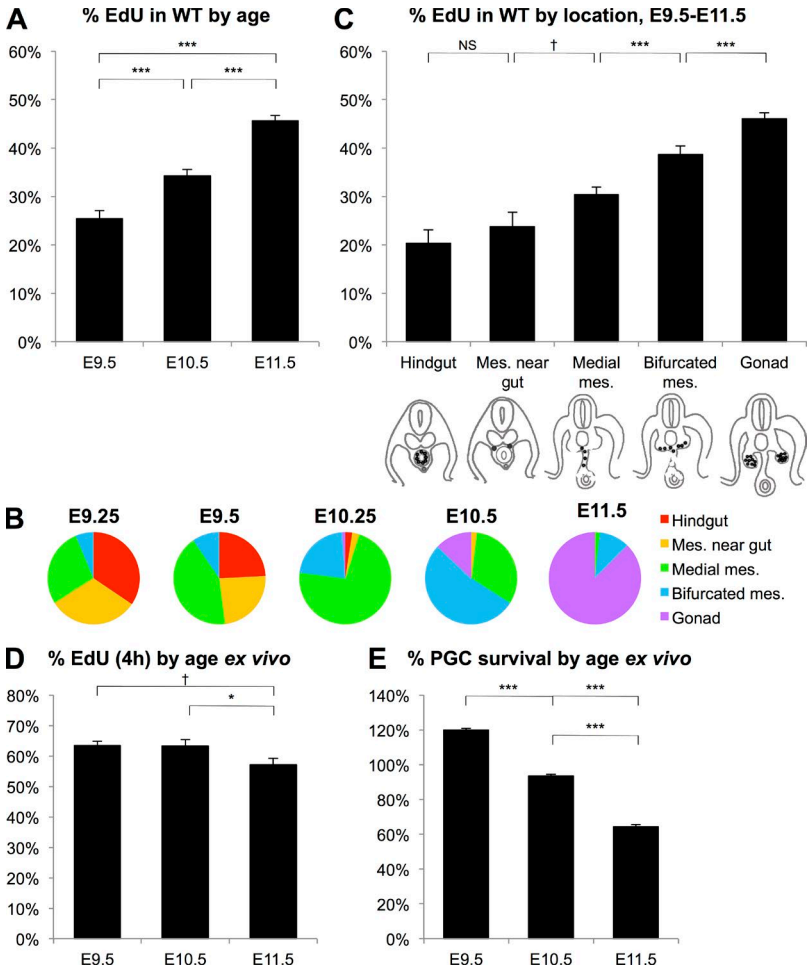

Figure 1. **Proliferation increases as PGCs move along their migratory route.** (A) The frequency of EdU incorporation in WT PGCs increases by age during the period of migration. n = 708–1,966 cells from 18 embryos; ***, P < 0.0001 by χ^2 and Fisher's exact test, χ^2 = 103.03, correlation coefficient = 0.998. (B) Distribution of PGCs by progressive location along the migratory route from the hindgut to three locations within the mesentery (mes.) to the gonad in combined ages E9.25 to E11.5. (C) The frequency of EdU incorporation in WT PGCs increases by location during migration. Anatomical cartoons show migratory PGCs as black dots. n = 197–1,817 cells from 18 embryos; †, P = 0.06 by Fisher's exact test; ***, P < 0.001 by χ^2 and Fisher's exact test; χ^2 = 116.19, correlation coefficient = 0.991. NS, not significant.(D) The frequency of EdU incorporation in WT PGCs cultured ex vivo is unaffected by age. n = 537–1,305 cells from four to eight experimental replicates; *, P = 0.04; †, P = 0.05 by Student's t test. (E) Survival of WT PGCs decreases by age when cultured ex vivo. n = 1189–2986 cells from 6 to 13 experimental replicates; ***, P < 0.001 by Student's t test; error bars in A, C, D, and E indicate standard error of the mean.

along the migratory route modulate the cell cycle in PGCs and perturbation of the noncanonical *Wnt5a–Ror2* pathway disrupts germ cell proliferation specifically in the hindgut. We identify *Wnt5a* as a key regulator of PGC proliferation through its ability to dampen canonical, *β-catenin*–mediated Wnt activity and observe that the in vivo Wnt response in PGCs correlates with their rate of division. Thus, we find a novel mechanism of niche-specific regulation of the cell cycle via the balance of antagonistic Wnt signaling pathways during germ cell development.

Results

PGC proliferation during migration is associated with location

Examination of PGCs through development previously identified a progressive increase in total number spanning the period from specification through sex differentiation (Tam and Snow, 1981; Seki et al., 2007). Subsequent analysis found that the rate of proliferation varied by embryonic age, with a slowing of the cell cycle around E9.0 (Seki et al., 2007). Using EdU incorporation to quantify cell proliferation (Fig. S1 A), we observed a similar relationship between the PGC cell cycle and embryonic age on a mixed genetic background (Fig. 1 A). However, because germ cell migration is largely individual and asynchronous, we noted that PGC locations were heterogeneous within a given embryonic age (Fig. 1 B). When indexed by location rather than age, the frequency of EdU$^+$ PGCs increased in each successive migratory compartment, from hindgut epithelium to gonadal ridge mesenchyme (P < 0.001 by χ^2, correlation coefficient = 0.991; Fig. 1 C). Importantly, this escalating rate of proliferation was observed within individual embryonic ages, particularly E9.5 and E10.5, where germ cell location is most diverse (Fig. S1, B–D). Additionally, the rate of proliferation remained largely constant in each location, irrespective of age. This trend held in C57BL6/CD1 embryos despite differing absolute levels of PGC proliferation (Fig. S1 E).

To assess the cell cycle of PGCs under controlled conditions, we turned to our previously established ex vivo culture, in which PGCs can be maintained free of feeder cells or serum for ∼24 h using defined medium and synthetic substrates (Laird et al., 2011). PGCs isolated at E9.5, E10.5, and E11.5 using the Oct4-ΔPE-GFP reporter (Anderson et al., 1999) were cultured in identical conditions. EdU analysis of these ex vivo cultures confirmed that PGC proliferation did not depend on age (Fig. 1 D). PGCs at E9.5 and E10.5 had identical rates of EdU incorporation, whereas the slight decrease in E11.5 PGCs is likely caused by the reduced cell survival in our culture conditions (Fig. 1 E). Thus, a correlation between the cell cycle rate and embryonic compartment in vivo suggests that location rather than intrinsic timing determines PGC proliferation.

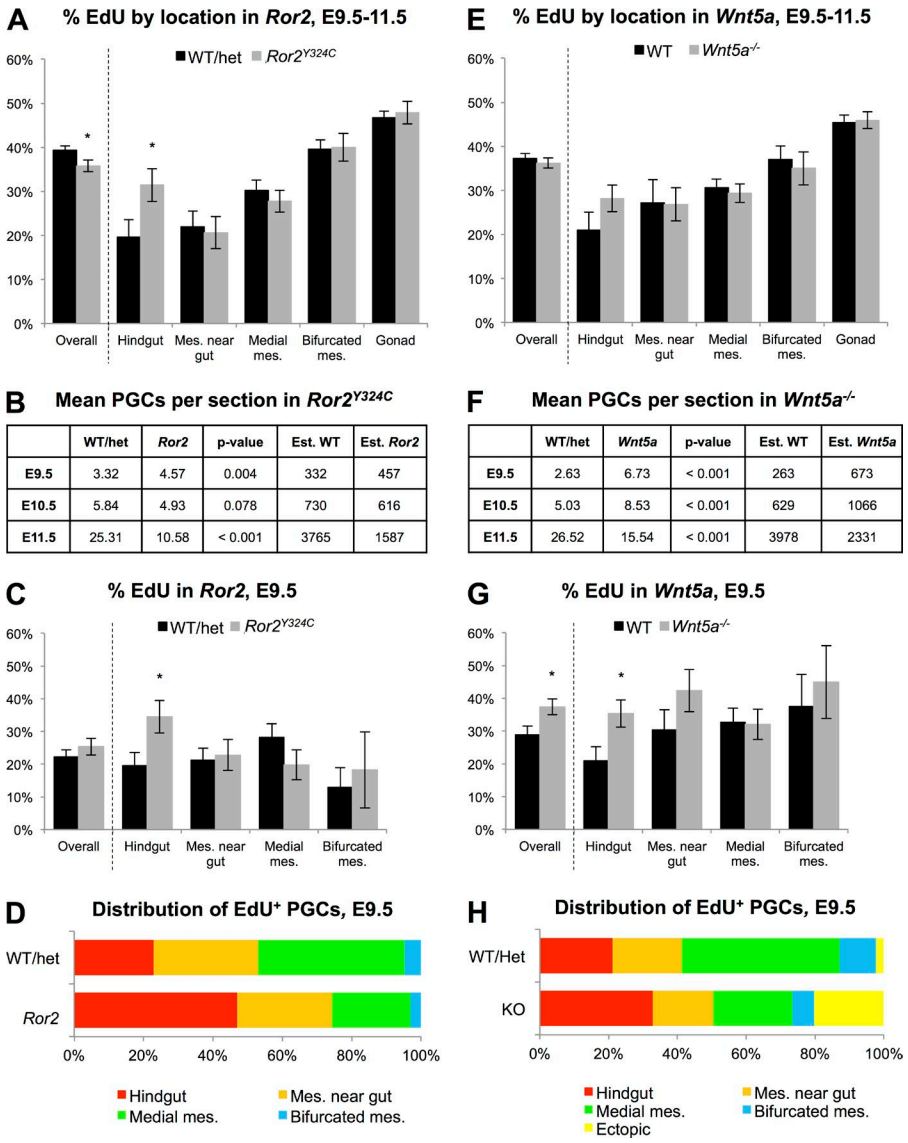

	WT/het	*Ror2*	p-value	Est. WT	Est. *Ror2*
E9.5	3.32	4.57	0.004	332	457
E10.5	5.84	4.93	0.078	730	616
E11.5	25.31	10.58	< 0.001	3765	1587

	WT/het	*Wnt5a*	p-value	Est. WT	Est. *Wnt5a*
E9.5	2.63	6.73	< 0.001	263	673
E10.5	5.03	8.53	< 0.001	629	1066
E11.5	26.52	15.54	< 0.001	3978	2331

Figure 2. **Removal of *Wnt5a* or *Ror2* disrupts PGC proliferation in distinct locations.** (A) The frequency of EdU incorporation is elevated in $Ror2^{Y324C}$ PGCs in the hindgut compared with WT or $Ror2^{Y324C/+}$ controls. EdU was given 4 h before dissection. *n* = 97–1,056 cells from nine WT/het embryos and ten mutant embryos; *, P = 0.04 by Fisher's exact test. (B) Mean number of PGCs counted in histological sections at different ages. P values by Student's *t* test for section counts. Estimates for total numbers of WT/het and $Ror2^{Y324C}$ PGCs per embryo were calculated using the multiplier of 100× for E9.5, 125× for E10.5, and 150× for E11.5 based on reported cell counts (Tam and Snow, 1981; Laird et al., 2011). (C) Frequency of EdU incorporation in E9.5 WT/$Ror2^{Y324C/+}$ PGCs and $Ror2^{Y324C}$ PGCs in different locations. *, P = 0.03 by Fisher's exact test. (D) Distribution of EdU+ PGCs by location at E9.5 in WT/$Ror2^{Y324C/+}$ PGCs and $Ror2^{Y324C}$ embryos. (E) Frequency of EdU incorporation in WT or $Wnt5a^{+/-}$ PGCs and $Wnt5a^{-/-}$ PGCs in different locations throughout migration. *n* = 70–761 cells from nine WT/het embryos and ten mutant embryos. (F) Mean number of PGCs counted in histological sections at different ages. P values by Student's *t* test for section counts. Estimates for total numbers of WT/het and $Wnt5a^{-/-}$ PGCs per embryo were calculated using the multiplier of 100× for E9.5, 125× for E10.5, and 150× for E11.5 based on reported cell counts. (G) Frequency of EdU incorporation in E9.5 WT/$Wnt5a^{+/-}$ PGCs and $Wnt5a^{-/-}$ PGCs in different locations throughout migration. *, P = 0.02 by Fisher's exact test. (H) Distribution of EdU+ PGCs by location at E9.5 in WT/$Wnt5a^{+/-}$ and $Wnt5a^{-/-}$ embryos. Error bars in A, C, E and G indicate standard error of the mean.

Disruption of noncanonical Wnt signaling alters PGC proliferation in the hindgut

Our hypothesis that proliferation of PGCs is environmentally regulated predicts that disrupting their localization should affect proliferation by age, but not location. Genetic mutants of the noncanonical Wnt receptor *Ror2* exhibit decreased efficiency of PGC colonization of the gonads (Laird et al., 2011). Although stragglers die in $Ror2^{Y324C/Y324C}$ ($Ror2^{Y324C}$) embryos, the restoration of normal germ cell number on a $Bax^{-/-}$ background indicates that migration is the primary defect (Laird et al., 2011). *Ror2* is broadly expressed in tissues critical for germ cell development, including somatic cells of the hindgut epithelium and surrounding dorsal mesentery (Yamada et al., 2010), as well as on migratory and postmigratory PGCs (Laird et al., 2011; Arora et al., 2014). As predicted, despite mislocalization of many $Ror2^{Y324C}$ germ cells from E9.5–11.5 (Fig. S2 A), the frequency of EdU incorporation was similar between wild-type (WT) and $Ror2^{Y324C}$ PGCs in the mesenchyme near the hindgut and subsequent mesentery and gonadal locations (Fig. 2 A). However, in the $Ror2^{Y324C}$ hindgut, PGCs did not cycle according to their location but instead showed an aberrant increase in EdU incorporation; concurrently, elevated numbers of PGCs per histological section at E9.5 (Fig. 2 B) were indicative of an expansion in the overall number of PGCs at this age. EdU incorporation showed an increase in the hindgut of $Ror2^{Y324C}$ mutants compared with WT at E9.5 (Fig. 2 C), but not at other locations or ages (Fig. S2, B and C), and the distribution of EdU-labeled PGCs at E9.5 was skewed toward the hindgut in $Ror2^{Y324C}$ rather than the mesentery as in WT (Fig. 2 D). These data suggest that Ror2 signaling restricts PGC proliferation exclusively within the hindgut.

Wnt5a is the primary ligand for *Ror2* (Hikasa et al., 2002; Oishi et al., 2003), and its expression along the PGC migratory route in the hindgut (Fig. S2 E), mesentery, and gonadal ridges (Laird et al., 2011; Fig. S3 E) coincides with expression of the *Ror2* receptor by PGCs (Laird et al., 2011). $Wnt5a^{-/-}$ embryos exhibit defects in the organization of the hindgut epithelium and reduced axial elongation (Yamaguchi et al., 1999; Cervantes et al., 2009). PGCs in these mutants migrate inefficiently (Fig. S2 D) and are diminished after E10.5 through an uptick in apoptosis (Laird et al., 2011; Chawengsaksophak et al., 2012). Our analysis of $Wnt5a^{-/-}$ embryos found a similar, but less severe, phenotype than in $Ror2^{Y324C}$; altered distribution of PGCs was associated with increased proliferation in the hindgut at E9.5 (Fig. 2 E,G), whereas no differences at other locations or

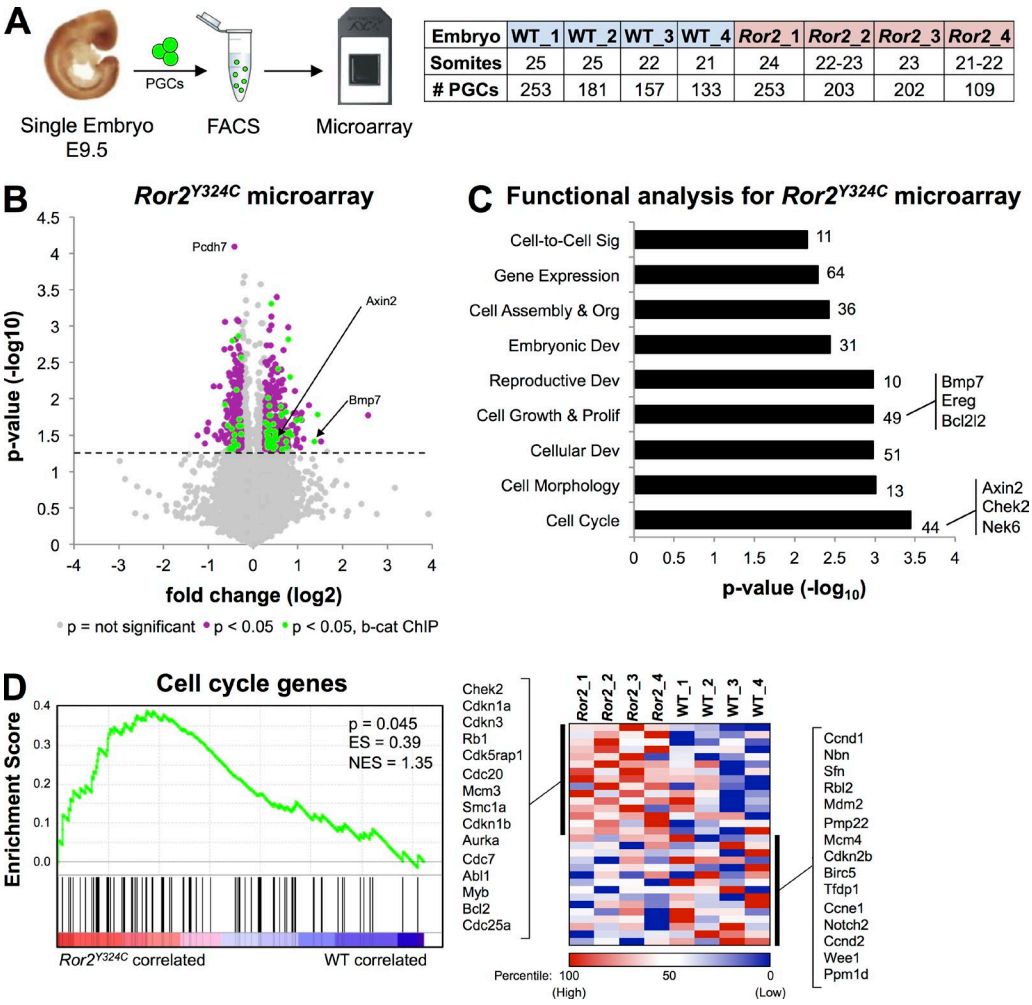

Embryo	WT_1	WT_2	WT_3	WT_4	Ror2_1	Ror2_2	Ror2_3	Ror2_4
Somites	25	25	22	21	24	22-23	23	21-22
# PGCs	253	181	157	133	253	203	202	109

Figure 3. ***Ror2^{Y324C}* downstream targets overlap with cell cycle–associated genes.** (A) Schematic of experimental design. Single embryos were collected at E9.5, and Oct4-ΔPE-GFP^{+} PGCs were isolated by FACS. RNA was extracted from WT (*Ror2$^{+/+}$*) and *Ror2^{Y324C}* PGCs, converted to cDNA, amplified, and hybridized to the GeneChip Mouse Gene 1.0 ST Array (Affymetrix). Age and number of PGCs collected per embryo are shown in the table. (B) Microarray data from *Ror2^{Y324C}* PGCs compared with WT shown as log fold change versus log p-values for all annotated microarray probes (dChip). Each dot represents a single probe. Purple dots show genes with a P < 0.05 and a fold change >1.2 (not log scale). Green dots show significant genes that overlap with *β-catenin* ChIP in mouse intestinal crypts (Schuijers et al., 2015). (C) Functional analysis of >1.2-fold microarray hits by Ingenuity Pathway Analysis find cell cycle–associated genes to be significantly misregulated. Number of genes associated with each Gene Ontology category is shown on the right. Exemplary genes of interest for cell cycle and cell growth and proliferation categories are listed. (D) GSEA comparison of the *Ror2^{Y324C}* microarray data with a curated list of cell cycle genes from the QIAGEN Cell Cycle PCR Array suggests an enrichment for *Ror2^{Y324C}*-associated genes. P-value, enrichment score (ES), and normalized enrichment score (NES) are specified. Heatmap shows normalized microarray intensity values for the 15 most and 15 least enriched cell cycle–associated genes in *Ror2^{Y324C}* PGCs as identified by the GSEA. For each gene, dark blue color indicates the lowest probe intensity value (zeroth percentile), dark red indicates the highest probe intensity value (100th percentile), and white indicates the middle 50th percentile of intensity values.

embryonic ages were found (Fig. S2, F and G). This observed uptick in proliferation in the E9.5 hindgut most likely leads to an increased number of PGCs per histological section in *Wnt5a$^{-/-}$* mutants at E9.5–10.5 (Fig. 2 F), corresponding to an overall increase in the PGC population at these ages. Strikingly, by E11.5, the number of PGCs per section was significantly decreased in both *Wnt5a* and *Ror2* mutants, consistent with the previously described loss through mismigration and subsequent apoptosis. Although our observations of *Wnt5a$^{-/-}$* confirmed the migratory phenotype of PGCs and ultimate reduction in their overall numbers (Laird et al., 2011; Chawengsaksophak et al., 2012), the altered distribution of proliferating *Wnt5a$^{-/-}$* PGCs in the hindgut and ectopic locations (Fig. 2 H) suggests that WNT5a levels calibrate early PGC mitosis. Thus, we conclude that *Wnt5a* in the hindgut signals through *Ror2* to limit PGC proliferation during migration.

Wnt5a-Ror2 regulates the PGC cell cycle via suppression of the canonical Wnt pathway

To identify the molecular mechanism connecting *Wnt5a–Ror2* signaling to the cell cycle in this lineage, we interrogated transcriptional changes in *Ror2^{Y324C}* PGCs from embryos at E9.5, when half or more are retained in the hindgut or nearby mesentery (Fig. 3 A). Microarray analysis of PGCs from single embryos showed significant misregulation of genes associated with the cell cycle and proliferation in the mutants (Fig. 3, B and C; Ingenuity Pathway Analysis). Gene set enrichment analysis (GSEA; Mootha et al., 2003; Subramanian et al., 2005) of this expression dataset with a curated list of cell cycle genes (Cell Cycle PCR Array; QIAGEN) confirmed that regulators of the cell cycle were overrepresented in genes associated with *Ror2^{Y324C}* PGCs (Fig. 3 D).

Examining specific changes in gene expression revealed no difference in levels of *Ror2* between the WT and mutant groups, corroborating previous findings that the *Ror2*^{Y324C} mutation is expressed but nonfunctional (Laird et al., 2011). Importantly, Ror family member *Ror1* was found to have very low (1/10th levels of *Ror2*) and unchanging expression in PGCs across groups, eliminating the possibility of compensation for loss of *Ror2* reported in other systems (Ho et al., 2012). Among >1.2-fold up-regulated transcripts in *Ror2*^{Y324C} PGCs was *Axin2*, an established target of the canonical Wnt pathway (Niehrs, 2012). *Ror2* has been linked to the suppression of canonical Wnt signaling using reporters of T-cell factor/lymphoid enhancer factor transcriptional activity (Mikels and Nusse, 2006; Mikels et al., 2009). To test this relationship, we generated compound mutants between *Ror2*^{Y324C} and a null allele of *β-catenin* (Brault et al., 2001). Although homozygous *β-catenin* deletion causes lethality at gastrulation (Haegel et al., 1995; Huelsken et al., 2000), PGCs from *Ror2*$^{Y324C/Y324C}$; *β-catenin*$^{+/-}$ embryos exhibited normal BrdU incorporation in ex vivo culture; this suggests that reduced dosage of *β-catenin* rescues the proliferation increase in *Ror2*^{Y324C} PGCs (Fig. S3 A). Together, these expression and genetic studies suggest that that *Ror2* opposes the *β-catenin*–dependent pathway in the regulation of PGC proliferation.

To explore the hypothesis that *β-catenin* acts downstream of *Ror2* signaling to regulate the cell cycle in migratory PGCs, we compared our microarray data from *Ror2*^{Y324C} PGCs to published data from *β-catenin* and *TCF1* chromatin immunoprecipitation (ChIP) sequencing. Because of a dearth of ChIP-sequencing data in PGCs, the most relevant and comprehensive dataset available was from the mouse intestinal crypt (Schuijers et al., 2015). Despite known discrepancies between cell lineages, we found that 13% of 1.2-fold changed genes from our microarray analysis (dChip; Li and Wong, 2001; or Ingenuity Pathway Analysis; QIAGEN) were also bound by *β-catenin* (Fig. S3 B). GSEA comparison of *β-catenin* ChIP peaks from mouse intestine showed a significant enrichment in genes associated with the *Ror2*^{Y324C} disruption in PGCs, including the targets *Axin2* and *Bmp7*, among others (Fig. S3 C). These data suggest links among *Wnt5a–Ror2*, the canonical Wnt pathway, and the PGC cell cycle.

WNT5a from somatic cells suppresses canonical Wnt/β-*catenin* activity in PGCs

The observed changes in proliferation highlight the influence of the somatic cell microenvironment on PGCs, whereas the *Ror2*^{Y324C} mutants implicate the canonical Wnt pathway in regulating their compartment-specific behaviors. To measure canonical Wnt responses in PGCs under controlled conditions, we returned to our ex vivo culture system using PGCs isolated from E9.5, when they reside largely in the hindgut and adjacent mesentery (Fig. 1 B). In the off state of signaling, cytoplasmic *β-catenin* is degraded by the *Axin–GSK3β–APC–CK1ε* complex (Logan and Nusse, 2004). However, engagement of Frizzled receptors by Wnt ligands causes dissociation of this complex and permits the accumulation and translocation of *β-catenin* to the nucleus, where it binds transcription factors in the T-cell factor/lymphoid enhancer factor family and induces gene expression (Niehrs, 2012). Therefore, levels of *β-catenin* protein in the nucleus reflect canonical Wnt pathway activation irrespective of ligands, receptors, or target genes (Behrens et al., 1996).

To model the embryonic hindgut and mesentery microenvironment, we compared levels of nuclear *β-catenin* (n-βcat) in E9.5 PGCs cultured with E9.5 tail somatic cells or in isolation (ISO; Fig. 4 A). After 20 h, we observed significantly diminished n-βcat in PGCs cocultured with soma (Fig. 4 B). Further, we saw that protein levels of *Axin2* (Yan et al., 2001; Jho et al., 2002; Lustig et al., 2002) and *E-cadherin*, another Wnt target gene (Jamora et al., 2003), were also decreased in PGCs cultured with somatic cells (Fig. 4, C and D). Whereas ISO PGCs exhibited relatively uniform levels of n-βcat, coculture with somatic cells produced a greater distribution in Wnt activity, suggesting a diversity of localized signaling environments within the culture dish (Fig. 4 E). The low density of cells in our culture suggested that secreted factors rather than cell contact dampens Wnt response in PGCs; accordingly, we found that conditioned media from E9.5 tail soma decreased n-βcat in ex vivo–cultured PGCs (Fig. 4 F). These results support the hypothesis that the hindgut and mesentery microenvironments suppress Wnt responses in PGCs.

To identify candidate ligands in relevant niches, we collected E-cad^{+}; Oct4-ΔPE-GFP^{-} hindgut cells and double negative mesentery cells from E9.5 tails (Bendel-Stenzel et al., 2000) as well as Oct4-ΔPE-GFP^{-} soma from isolated gonadal ridges (Fig. S3 D). Somatic cells in the hindgut (E9.5 Ecad^{+}) expressed Wnt antagonists *Wnt5a* and *Dkk1*, whereas the gonadal ridge soma expressed *Wnt5a* and high levels of *Sfrp1* (Fig. S3 E). Abundance of *Dkk1* and *Sfrp1* in the E9.5 Ecad^{-} population was intermediate, suggesting that the mesenchyme surrounding the hindgut is a transitional zone during PGC migration.

Based on the genetic evidence that Wnt5a suppresses proliferation within the hindgut and molecular association between *Ror2* and *β-catenin* targets, we pursued *Wnt5a* as a candidate secreted regulator of canonical Wnt signaling in PGCs. Exogenous WNT5a reduced levels of n-βcat in WT, E9.5 PGCs similarly to our tail somatic cells (Fig. 5 A), but the relatively uniform response suggested increased consistency throughout the culture environment. In contrast to WT, *Ror2*^{Y324C} PGCs cultured with exogenous WNT5a did not dampen the Wnt response and instead activated the canonical pathway (Fig. S3 F). This suggests that *Wnt5a* acts primarily through the *Ror2* receptor to inhibit *β-catenin*–dependent signaling, but when *Ror2* is nonfunctional, Wnt5a signals through other receptors on PGCs.

To verify that altered levels of n-βcat correspond to transcriptional changes in our system, we interrogated expression of putative canonical Wnt target genes in ex vivo–cultured PGCs. After PGC culture in the presence of WNT5a, qRT-PCR revealed a decrease of several Wnt target transcripts established in other cell types including *Axin2*, *Cdh1*, *Fn1*, and *Lef1* (Fig. 5 B); importantly, levels of the germ cell gene *Dppa3* (*Stella*) remained unaffected. Accordingly, we found that *E-cadherin* (*Cdh1*) protein was reduced in PGCs treated with WNT5a (Fig. 5 C). These results confirm that changes in Wnt target gene transcription accompany changes in n-βcat observed in PGCs.

Although the aforementioned experiments show that WNT5a suppresses canonical Wnt activity in PGCs, they do not validate its relevance as a mediator of this suppression by somatic cell populations. Because of the expression of Wnt inhibitor *Dkk1* in the hindgut and tail mesentery, we performed loss-of-function studies with mouse embryonic fibroblasts (MEFs) that express *Wnt5a* (Fig. S3 E) and produce a similar reduction in n-βcat of PGCs (Fig. 5 D) but have undetectable levels of *Dkk1*. Coculture of E9.5 PGCs with *Wnt5a*$^{-/-}$ MEFs alleviated the suppression of n-βcat observed with WT MEFs and led to increased Wnt response over that of isolated PGCs

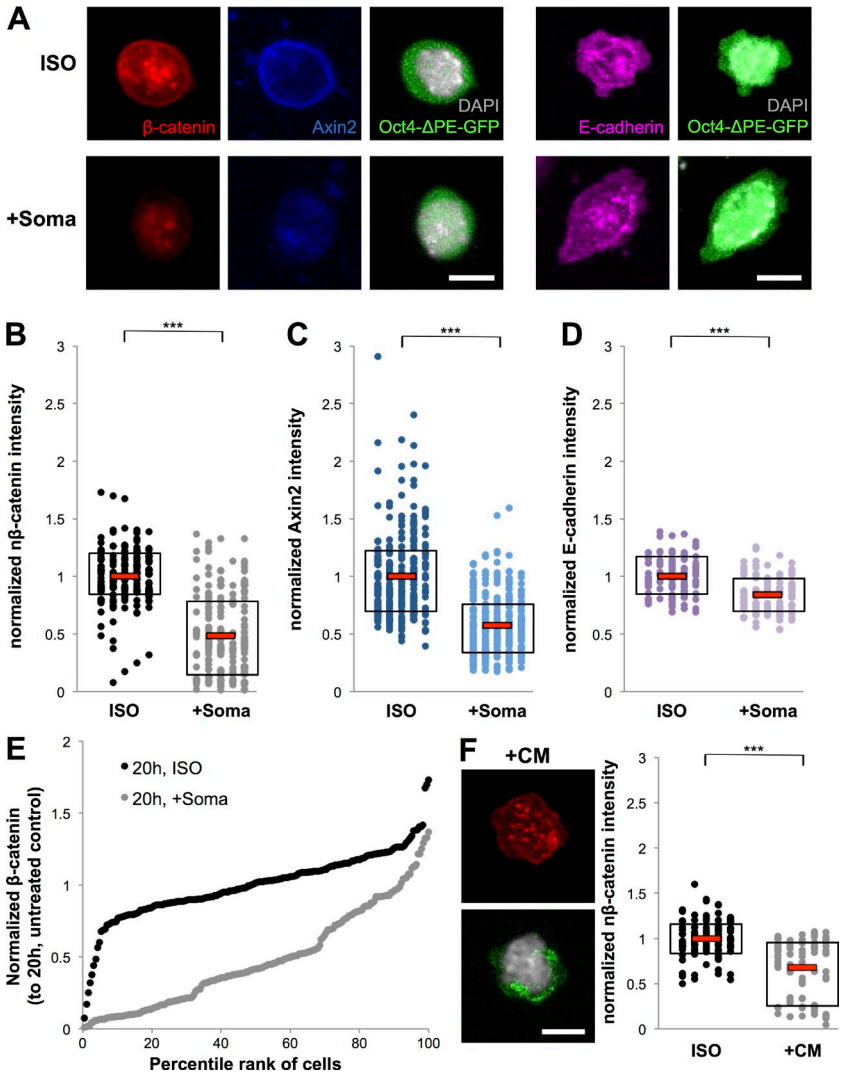

Figure 4. **Somatic cells suppress Wnt/*β-catenin* activity in PGCs.** (A) Nuclear *β-catenin* (n-βcat, red), *Axin2* (blue), and *E-cadherin* (magenta) immunofluorescence in E9.5 PGCs (green) cultured for 20 h in isolation (ISO) or with E9.5 tail somatic cells (+Soma) from tail somatic cells. Images are representative of mean values. Bar, 10 µm. (B) Quantification of n-βcat in cultured PGCs from A. n-βcat intensity for each PGC is normalized to the mean value of PGCs cultured in isolation in the same experiment. Each dot represents a single PGC; bars indicate the mean and boxes denote the middle 50% of data points. $n = 3$ experiments, 186–203 cells per condition; ***, $P < 0.001$ by Student's *t* test. (C) Quantification of Axin2 in cultured PGCs from A. AXIN2 intensity for each PGC is normalized to the mean value of PGCs cultured in isolation in the same experiment. $n = 4$ experiments, 293–309 cells per condition; ***, $P < 0.001$ by Student's *t* test. (D) Quantification of E-cadherin in cultured PGCs from A. E-CADHERIN intensity for each PGC is normalized to the mean value of PGCs cultured in isolation. $n = 2$ experiments, 102–114 cells per condition; ***, $P < 0.001$ by Student's *t* test. (E) Percentile rank of individual cell n-βcat from B. (F) n-βcat (red) immunofluorescence in E9.5 PGCs (green) cultured for 20 h in isolation (ISO) or with conditioned media (+CM) from E9.5 tail somatic cells. Bar, 10 µm. Graph shows quantification of n-βcat in PGCs in these conditions. $n = 4$ experiments, 84–112 cells per condition; ***, $P < 0.001$ by Student's *t* test.

(Fig. 5 D). Moreover, the addition of exogenous WNT5a to the *Wnt5a*$^{-/-}$ MEF cocultures restored this suppression and reduced n-βcat in the PGCs. Thus, we conclude that *Wnt5a* secreted from somatic cells in the hindgut and surrounding mesenchyme serves to suppress canonical Wnt activity in migratory PGCs.

Specific somatic compartments modulate the canonical Wnt response in migratory PGCs

To assess canonical Wnt response at a single-cell level in vivo, we developed a protocol to quantitatively image and measure n-βcat in histological sections. After enzymatic treatment to render the nucleus accessible (Fig. S4 A), we measured the mean n-βcat immunofluorescence signal intensity within PGCs as compared with the mean intensity across all nuclei in an image (Fig. 6 A). This normalization enabled comparison of n-βcat intensity between histological sections and between slides.

On applying this method to sections from *Ror2*^{Y324C} embryos at E9.5, we found that overall levels of n-βcat in PGCs were higher than in WT (Fig. 6 B). This was also true when the data were separated by location (Fig. 6 C), consistent with elevated Wnt target genes in *Ror2*^{Y324C} microarray data. By E10.5, this increase in overall accumulation of n-βcat in *Ror2*^{Y324C} PGCs returned to WT levels (unpublished data), suggesting that overactive Wnt signaling is not sustained throughout the migratory period and supporting the decrease in overall proliferation at this age (Fig. S2 B).

To assess Wnt signaling in PGCs across embryonic ages, we studied WT embryos, in which we observed a wide range in levels of n-βcat, the highest being at E11.5 (Fig. S4 B). Mean n-βcat in PGCs in the E12.5 testis was comparatively low, reflecting the established repression during male sex differentiation (Chassot et al., 2011). Despite fluctuation of n-βcat in PGCs by age, the higher population mean in post-migratory PGCs at E11.5 compared with E9.5 (Fig. S4 B) again prompted our examination by location. From E9.5 to E11.5, we observed a progressive increase in n-βcat at each successive migratory location from the hindgut to the gonadal ridge ($R^2 = 0.97$ and $P = 0.002$ by regression analysis; Fig. 6 D). This pattern was retained at single ages, with lower levels of n-βcat in PGCs in the hindgut and adjacent mesenchyme compared with PGCs in mesentery or gonadal tissues (Fig. S4, C and D). PGC n-βcat did not vary with rostral-caudal position in the embryo (unpublished data), suggesting that a consistent environment within each compartment regulates the Wnt response in PGCs. In a striking parallel to our initial proliferation studies, this result corroborates the idea that the local environment, rather than intrinsic timing, determines canonical Wnt responses in PGCs.

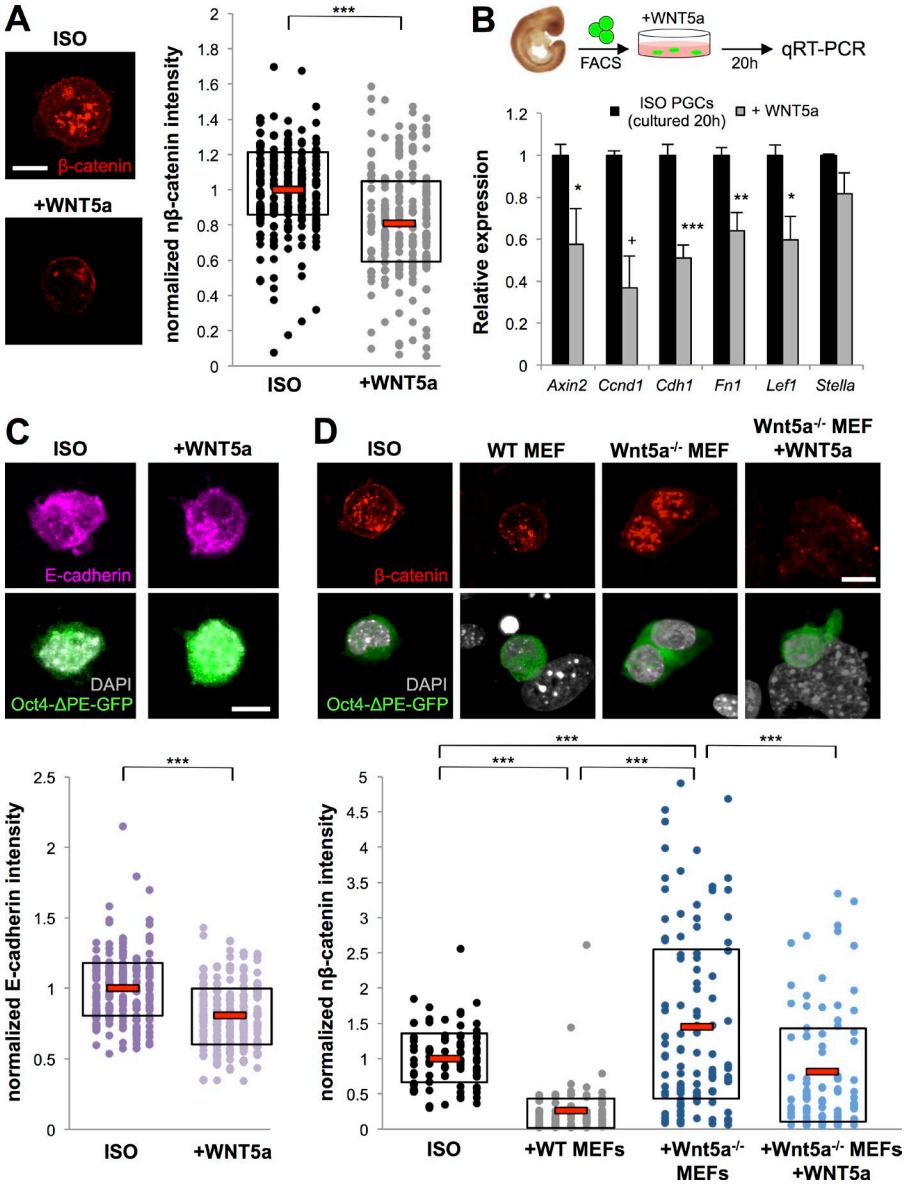

Figure 5. ***Wnt5a* secreted by somatic cells suppresses canonical Wnt signaling in PGCs.** (A) n-βcat (red) in E9.5 PGCs cultured for 20 h in isolation (ISO) or with exogenous WNT5a (250 ng/ml). Bar, 10 µm. Quantification shows reduced n-βcat in individual PGCs in presence of WNT5a. Each dot represents a single PGC; bars indicate the mean and boxes denote middle 50% of data points. *n* = 3 experiments, 244–254 cells per condition; ***, P < 0.001 by Student's *t* test. (B) Expression of candidate Wnt targets by qRT-PCR in ex vivo cultured E9.5 PGCs from A decreases in the presence of WNT5a. Results are normalized to the mean of *Gapdh/Rpl7* and presented relative to ISO control. ***, P < 0.001; **, P < 0.01; *, P < 0.05; +, P = 0.052 by Student's *t* test; error bars indicate standard error of the mean. (C) *E-cadherin* (*Cdh1*, magenta) immunofluorescence in E9.5 PGCs cultured for 20 h. Images are representative of mean values. Bar, 10 µm. Quantification confirms reduced expression of E-CADHER IN in the presence of WNT5a. *n* = 3 experiments, 212–231 cells per condition; ***, P < 0.001 by Student's *t* test. (D) n-βcat (red) in E9.5 PGCs (green) cultured 20 h in isolation, with WT MEFs, *Wnt5a*$^{-/-}$ MEFs, or *Wnt5a*$^{-/-}$ MEFs plus exogenous WNT5a. Bar, 10 µm. Quantification of n-βcat in individual PGCs shows absence of suppression by *Wnt5a*$^{-/-}$ MEFs that is restored with exogenous WNT5a. *n* = 3 experiments; 86–104 cells each; ***, P < 0.001 by analysis of variance.

Genetic manipulation of β-*catenin* levels in PGCs alters proliferation

The parallel trajectories of proliferation and n-βcat together with the *Wnt5a* and *Ror2* mutant defects suggest that suppression of canonical Wnt signaling slows proliferation during early PGC migration. To test this hypothesis, we bypassed the antagonistic effects of the hindgut and mesentery by over-activating *β-catenin* in migratory PGCs. We crossed mice carrying a gain-of-function (GOF) allele (Harada et al., 1999), *β-catenin*$^{floxE3/floxE3}$, to mice with a drug-inducible Cre recombinase inserted into the *Oct4* locus (Greder et al., 2012), *Pou5f1*$^{Cre\text{-}ER/+}$. Tamoxifen administration at E7.75 or E8.25 of pregnancy induced excision of *β-catenin* exon 3, preventing degradation of the protein in PGCs (Fig. 7 A). Because of widespread expression of Oct4 through E7.5 (Downs, 2008), we tested this tamoxifen schedule in *Rosa*^{mTmG} reporter mice (Muzumdar et al., 2007) crossed to *Pou5f1*$^{Cre\text{-}ER/+}$ and observed overall specificity for excision in PGCs compared with their surrounding somatic tissues (Fig. S5 A). After activation of the *Pou5f1*$^{Cre\text{-}ER}$ allele, the resulting *β-catenin*^{GOF} embryos exhibited an increase in the number of PGCs per section at E9.5 when compared with Cre-negative littermates (Fig. 7, B and C). No difference was observed in the frequency of apoptotic PGCs in mutants (unpublished data).

Examination of proliferation by EdU incorporation in vivo did not reveal differences in labeled PGCs in *β-catenin*^{GOF} mutants (Fig. S5 C). Curiously, EdU labeling was aberrantly high in the control PGCs relative to PGCs in mice of mixed genetic background (Fig. 1 C), suggesting that cell cycle is altered by exposure to tamoxifen or differs in the C57BL6 background as compared with mixed background controls. To circumvent this issue and improve temporal control over the timing of excision, we cultured E9.5 PGCs from single *Pou5f1*$^{Cre\text{-}ER/+}$; *Oct4-ΔPE-GFP*$^{tg/+}$; *β-catenin*$^{floxE3/+}$ embryos with their corresponding WT tail soma to simulate the Wnt-suppressive in vivo environment. After adding 4OH-tamoxifen (Fig. 7 A), we observed a similar frequency of EdU incorporation after 10 h in culture. However, by 17 h, PGCs from Cre^{+} (GOF) embryos exhibited an increased proliferation rate over PGCs from controls (Fig. 7 D), suggesting that intrinsic overactivation of the canonical Wnt pathway allows PGCs to bypass the suppression

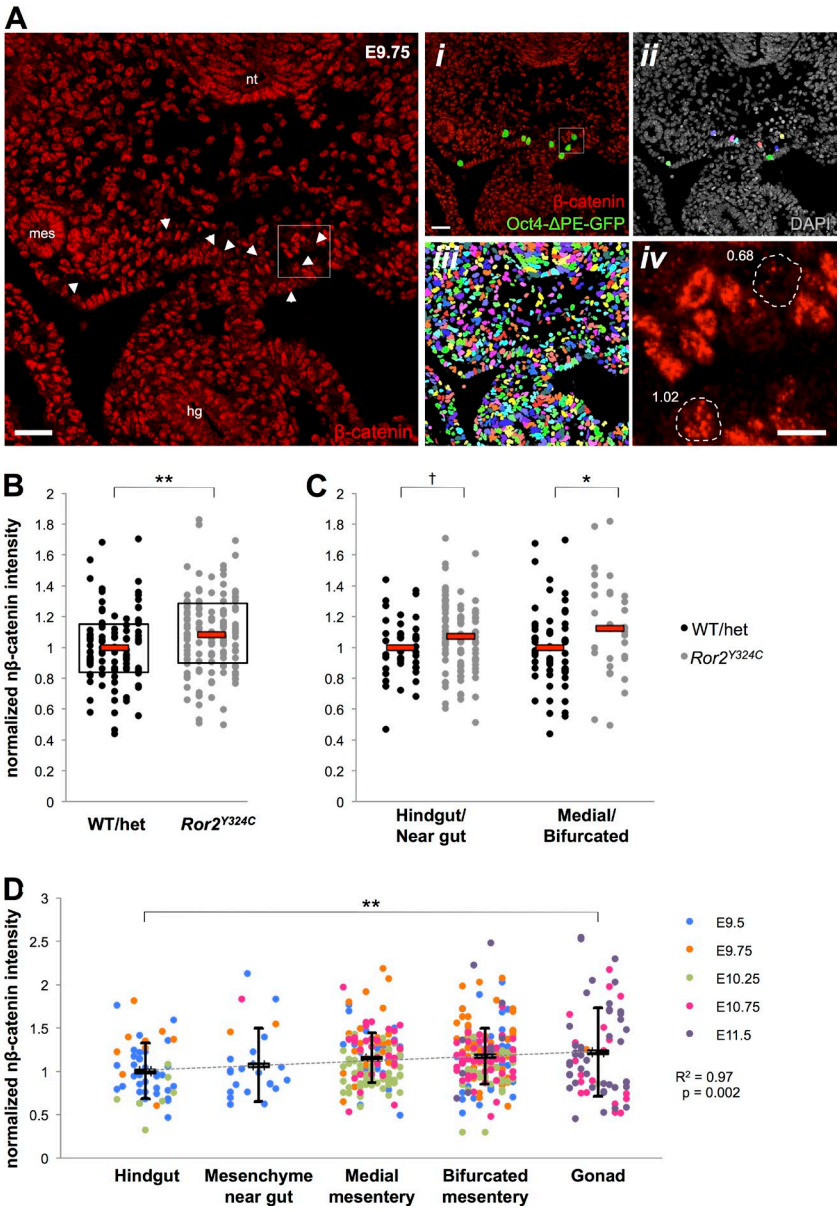

Figure 6. **Increased nuclear *β-catenin* levels in PGCs during their migratory progression and perturbation in *Ror2*^{Y324C} PGCs.** (A) Nuclear *β-catenin* (n-βcat, red) immunofluorescence in transverse histological sections of an E9.75 WT embryo treated with Ficin enzyme to disrupt *E-cadherin/β-catenin* membrane staining. The hindgut (hg), neural tube (nt), and mesonephric duct (mes) are indicated. Bar, 30 µm. (i) PGCs are identified by expression of Oct4-ΔPE-GFP (green; white arrows in A). Bar, 30 µm. (ii) Pseudocoloring (rainbow) indicates individually selected Oct4-ΔPE-GFP^{+} PGCs for quantitative measurement of n-βcat. (iii) Pseudocoloring (rainbow) indicates DAPI-selected nuclei of all cells in the field (>600 counted) used to obtain the mean intensity of n-βcat. (iv) Inset from box in A and i to exemplify differences in n-βcat levels in PGCs (dashed white lines) relative to the mean n-βcat levels in all nuclei in the field. Fold differences in staining intensity are indicated. Bar, 10 µm. (B) Quantification of n-βcat in all E9.5 *Ror2*^{Y324C} PGCs relative to WT/het littermates shows an increase in accumulation of n-βcat. Each dot represents a single PGC; bars indicate the mean and boxes denote the middle 50% of data points. n = 100–134 cells from two embryos per group; **, P < 0.01 by Student's t test. (C) Quantification of n-βcat in E9.5 PGCs from B by location. *, P = 0.045; †, P = 0.074 by Student's t test. (D) Quantification of n-βcat in migratory PGCs at various anatomical locations in E9.5–11.5 embryos. n-βcat in PGCs is normalized to mean n-βcat in surrounding nuclei as described in A and shown relative to the hindgut. Each dot represents a single PGC, and bars indicate the mean ± standard deviation. The dotted line indicates a trend of increasing n-βcat with migratory location. n = 25–203 cells per location from ten mixed CD1 embryos. R^2 = 0.97; P = 0.002 by regression analysis; P = 0.009 by analysis of variance; **, P = 0.009 by Student's t test.

by neighboring somatic cells. This result corroborates the uptick in overall numbers of PGCs counted at E9.5–10.5 in vivo (Fig. 7 B). Thus, ectopic activation of the canonical Wnt pathway in migratory PGCs is sufficient to alter their proliferation in environments associated with early stages of migration. Interestingly, our cumulative data show a mislocalization of PGCs along the migratory route of GOF mutants, indicative of a migration defect (Fig. S5 B); this concomitant perturbation of migration and proliferation is consistent with PGC phenotypes in *Wnt5a* and *Ror2* mutants and the antagonism between *β-catenin* and *Wnt5a–Ror2* pathways.

To further interrogate this relationship, we conducted genome-wide transcriptional analysis on E9.5 *β-catenin*^{GOF} PGCs from single embryos. Similar to our microarray results in *Ror2*^{Y324C} PGCs, misregulated genes in *β-catenin*^{GOF} PGCs comprised *Axin2* as well as gene sets associated with several cell cycle–related functions, including DNA replication and repair, proliferation, cell growth, and cell death and survival (Fig. 7, E and F). This parallel between datasets was strengthened by the identification of 35% overlap in the specific genes that are misregulated by each mutation (Fig. 7 G). Further, GSEA comparison of *β-catenin*^{GOF} gene targets in PGCs with our *Ror2*^{Y324C} expression dataset revealed an enrichment of genes associated with both mutations (Fig. 7 H). Together with in vivo phenotypic similarities, these bioinformatic correlations identify antagonistic functions for *Ror2* and *β*-catenin–mediated signaling in the regulation of PGC proliferation and migration.

Discussion

Here, we examined the proliferation of PGCs during migration and showed that their expansion is regulated by the somatic compartments through which they move. We identified canonical Wnt signaling as a mechanism that controls this proliferation and the *Wnt5a–Ror2* axis as a key suppressor of Wnt activity during transit through the hindgut and surrounding mesenchyme (Fig. 8). We observed a steady rise in the PGC Wnt response along the migratory route, concomitant with increased cycling, and demonstrated that excessive proliferation

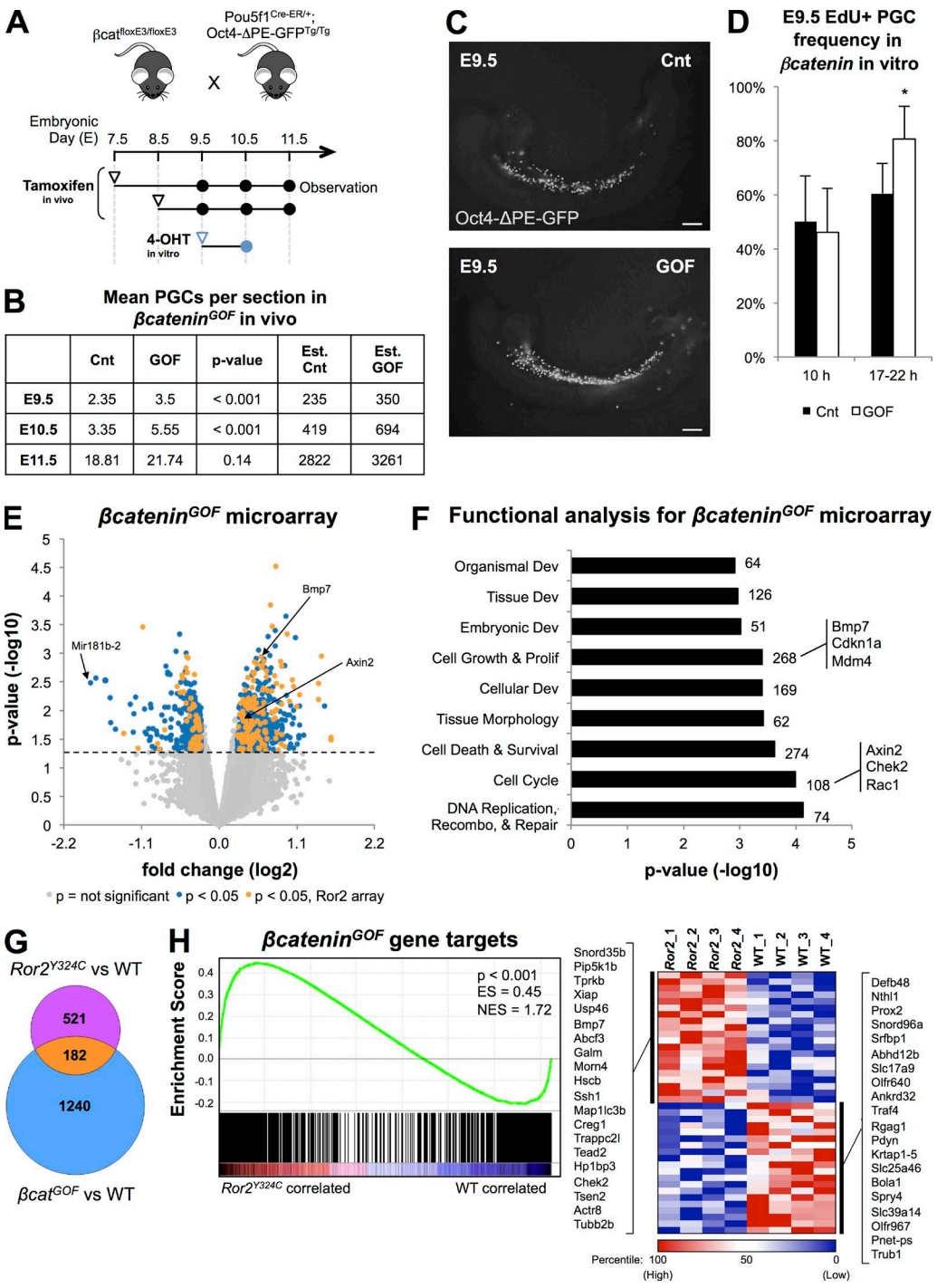

Figure 7. **Overactivation of *β-catenin* in PGCs leads to an increase in proliferation and misregulation of genes in common with *Ror2*^{Y324C}.** (A) Schematic of breeding and tamoxifen exposure to generate control (Cnt, *β-catenin*$^{GOF/+}$; *Pou5f1*$^{+/+}$) and *βcat*^{GOF} (*β-catenin*$^{GOF/+}$; *Pou5f1*$^{Cre\text{-}ER/+}$) embryos in vivo and cells ex vivo. (B) Mean number of PGCs counted in histological sections of Cnt and *βcat*^{GOF} embryos at different ages. *n* = 13 Cnt embryos and 15 *βcat*^{GOF} embryos. P-values by Student's *t* test for section counts. Estimates for total numbers of Cnt and *βcat*^{GOF} PGCs per embryo were calculated using the multiplier of 100× for E9.5, 125× for E10.5, and 150× for E11.5 based on cell counts reported in the literature. (C) Oct4-ΔPE-GFP^{+} PGCs (gray) in E9.5 littermates. Bar, 100 μm. (D) Rate of in vitro EdU incorporation in Cnt and *βcat*^{GOF} PGCs cultured for 10–22 h with 4-OHT. *n* = 4 litters; 794–818 cells; *, P < 0.05 by Student's *t* test; error bars indicate standard deviation. (E) Microarray data from *βcat*^{GOF} PGCs compared with WT shown as log fold change versus log p-values for all annotated microarray probes (Gladstone Bioinformatics Core [GBC]). Each dot represents a single probe. Blue dots show genes with P < 0.05 and a fold-change >1.2 (not log scale). Orange dots show significant genes that overlap with *Ror2*^{Y324C} misregulated genes. (F) Functional analysis of >1.2-fold microarray hits by Ingenuity Pathway Analysis find cell cycle–associated genes to be significantly misregulated. Number of genes associated with each Gene Ontology category is shown on the right. Example genes of interest for cell cycle and cell growth and proliferation categories are listed. (G) Number of genes that overlap between *Ror2*^{Y324C} microarray hits (dChip) and *βcat*^{GOF} microarray hits (GBC). (H) GSEA comparison of the *Ror2*^{Y324C} microarray dataset with *βcat*^{GOF} misregulated genes suggests an enrichment for genes associated with both mutations. P-value, enrichment score (ES), and normalized enrichment score (NES) are specified. Heatmap shows normalized microarray intensity values for the 20 most and 20 least enriched genes in *Ror2*^{Y324C} PGCs that are misregulated in the *β-catenin*^{GOF} microarray dataset. For each gene, dark blue color indicates the lowest probe intensity value (zero percentile), dark red indicates the highest probe intensity value (100th percentile), and white indicates the middle 50th percentile of intensity values.

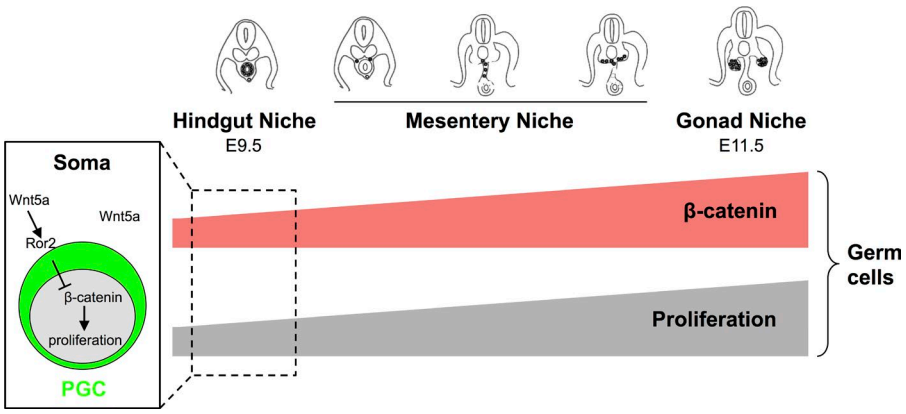

Figure 8. **Model of results.**

during early PGC migration can be induced by autonomously over-activating *β-catenin*. Together, these results identify a yin and yang of Wnts in proliferation and migration: canonical Wnt signaling drives the expansion of migratory PGCs, counterbalanced in specific niches by *Wnt5a–Ror2*, which promotes their movement.

Previous examination of the *Wnt5a*$^{-/-}$ and *Ror2*^{Y324C} mutants identified defects in the migration and survival of PGCs (Laird et al., 2011; Chawengsaksophak et al., 2012). Our current studies have uncovered an additional role for these genes in regulating PGC proliferation during the early and most active stages of their migration. Historically, Wnt5a is considered a noncanonical Wnt ligand (Moon et al., 1993; Wong et al., 1994); however, recent work in vivo has demonstrated its capacity to activate or antagonize the canonical Wnt pathway in a tissue-specific context (van Amerongen et al., 2012). Proposed mechanisms for *Wnt5a*-induced attenuation of the canonical Wnt pathway include competition for binding Frizzled receptors, simultaneous engagement of different receptors, and blocking transcription downstream of *β-catenin* (Mikels and Nusse, 2006; Yamamoto et al., 2008; Sato et al., 2010). This final mechanism is ruled out in PGCs by our observation that decreased n-βcat levels accompany diminished Wnt target transcripts after WNT5a treatment.

Our studies confirm that *Ror2* is the relevant receptor for mediating *Wnt5a*-induced attenuation of *β-catenin*–dependent signaling in migratory PGCs, consistent with previous biochemical studies (Mikels and Nusse, 2006). The permissive role of *Wnt5a* in PGC migration (Laird et al., 2011), together with its repression of proliferation, leads to the model that *Wnt5a* acts through *Ror2* to balance the promotion of PGC movement while limiting mitosis. This balance may be particularly important for known periods of active migration, such as egress from the hindgut, which is when we observe the strongest effect. Considering the potential conflicts posed to migration by cell division (loss of adhesion and orientation, as well as spatial constraints in tightly packed tissue), negotiation of both by *Wnt5a–Ror2* offers a single solution. The identification of *Wnt5a* and *Ror2* as prognostic biomarkers for tumor invasiveness (Weeraratna et al., 2002; Edris et al., 2012; Lu et al., 2012) raises the possibility that cancer cells exploit the same mechanism to regulate metastasis and growth.

Our study identifies the Wnt pathway as a mechanism for extrinsic regulation of proliferation in migratory PGCs. Previous work demonstrated a mitogenic role for *KitL–cKit* in PGCs, and dynamic expression of *KitL* in somatic compartments of the migratory route provides temporal specificity of signaling in each niche (Runyan et al., 2006; Gu et al., 2009). Prior studies also identified the chemokine SDF1 as a potential mitogen for PGCs primarily in the gonad (Ara et al., 2003; Molyneaux et al., 2003). Both pathways may function redundantly with Wnt signaling to regulate PGC proliferation during migration. Redundancy in the control of PGC division may have arisen as an advantage in the face of consequences for reproduction: sterility from insufficient PGCs or germ cell tumors from their unchecked proliferation. "Agreement" between multiple mechanisms of cell cycle control in PGCs may have evolved to prevent tumor formation and safeguard against overrepresentation of germline variants with elevated proliferation (Burt and Trivers, 2006). However, our data suggest that in a WT context, the balance between migration and proliferation could serve as a selective mechanism to reward early and efficient migrators—"pioneer" germ cells (Gomperts et al., 1994)—with clonal dominance in the ensuing germ cell pool, while penalizing stragglers with reduced time for expansion.

PGCs interact with a diversity of tissues as they move from the developing endoderm to the gonadal ridges yet are able to retain their germ cell characteristics. Migration through these microenvironments supports their survival, regulates their proliferation, and maintains their unique pluripotency program. Wylie et al. proposed that PGCs thus migrate along a "traveling niche," which provides a spatiotemporal environment analogous to a stem cell niche that maintains germ cell properties despite spanning diverse regions of the embryo (Gu et al., 2009). The departure from this niche by mismigration leads to either cellular demise or loss of PGC identity through transformation to pluripotent embryonic carcinoma cells (Matsui et al., 1992; Resnick et al., 1992). Our data suggest that WNT5a is a component of this dynamic niche, maintaining the migratory capability of PGCs while balancing their proliferation; however, it is likely that additional factors modulate the *β-catenin*–dependent response in PGCs. The expression of multiple and varied Wnt regulators by the somatic environment is suggested by the elevated Wnt response in WT gonadal PGCs (Fig. 6 D), increased n-βcat in PGCs cocultured with *Wnt5a*$^{-/-}$ MEFs (Fig. 5 D), and differences in cell cycle response by location despite similar overactivation of Wnt signaling in E9.5 *Ror2*^{Y324C} PGCs (Fig. 6 C). Other Wnt ligands with known expression in the embryonic posterior or in tissues of the PGC migratory route include *Wnt3a* (Takada et al., 1994), *Wnt4* (Vainio et al., 1999), and *Wnt11* (Kispert et al., 1996). Interactions between alternative Wnt modulatory factors may also be important. For example, WNT5a in the gonad could be neutralized by high levels of SFRP1 (Fig. S3 E) to enable robust canonical Wnt activity

in PGCs. We speculate that the expansion of migratory PGCs is achieved by calibration of their canonical Wnt activity in each somatic compartment by a distinct composition of activators and inhibitors. Our investigation into the dynamic microenvironment of migratory PGCs using ex vivo, coculture approaches paves the way for further characterization of each embryonic compartment and the cellular interactions between PGCs different somatic cell populations.

The balancing regulation of motility and proliferation by the microenvironment through noncanonical and canonical Wnt pathways may function similarly in other itinerant cell lineages in development, such as hematopoietic stem cells and neural crest. Further exploration of these microenvironments at both the cellular and mechanistic levels will enhance understanding of the interplay between migration of precursor populations and other simultaneous cell processes critical to their development.

Materials and methods

Animals

WT embryos were generated by mating CD1 females with homozygous Oct4-ΔPE-GFP males (MGI:3057158, multiple-copy transgene insertion; Anderson et al., 1999). Other mouse strains were maintained on a mixed or C57BL6 background, including: *Ror2*^{Y324C} (MGI:5305088, ENU-induced point mutation; Laird et al., 2011), *Wnt5a* (MGI:1857617, targeted deletion; Yamaguchi et al., 1999), *Pou5f1*$^{Cre\text{-}ER/+}$ (MGI:5049897, targeted knockin; Greder et al., 2012), *Rosa*^{mTmG} (MGI:3716464, targeted knockin; Muzumdar et al., 2007), and *β-catenin*^{floxE3} (MGI:1858008, targeted floxed allele; Harada et al., 1999). *β-catenin*$^{+/-}$ mice were created by crossing *β-catenin*$^{floxE2\text{-}6}$ mice (MGI:2148567, targeted floxed allele; a gift from K. Hadjatonakis (Memorial Sloan Kettering Cancer Center, New York, NY); Brault et al., 2001) to *Zp3*$^{cre/+}$ (MGI:2176187, transgene insertion; de Vries et al., 2000) for germline deletion.

Embryos were dissected from timed matings and staged by the following anatomical landmarks: 20–25 somite pairs was designated E9.5, 26–28 as E9.75, 30–33 as E10.25, 34–37 as E10.5, 38–41 as E10.75, and 45–48 somite pairs and defined limb morphology as E11.5 (Kaufman, 1992). Genotypes were determined by PCR. All mouse work was performed under the University of California, San Francisco, Institutional Animal Care and Use Committee guidelines in an approved facility of the Association for Assessment and Accreditation of Laboratory Animal Care International.

Tamoxifen and EdU injections

To generate *β-catenin* GOF PGCs, *β-catenin*$^{floxE3/floxE3}$ females were mated with *Pou5f1*$^{Cre\text{-}ER/+}$; *Oct4-ΔPE-GFP*$^{tg/tg}$ males. Tamoxifen (#T5648; Sigma-Aldrich) was suspended at 20 mg/ml in sunflower seed oil (#S5007; Sigma-Aldrich) and administered via intraperitoneal injection on day E7.75 at 5 mg/30g mouse weight. 4-Hydroxytamoxifen (#H7904; Sigma-Aldrich) was added at 1 µM to cells in culture at 0–3 h after seeding.

EdU (#C10338, Click-It Imaging kit; Thermo Fisher Scientific) was suspended at 2.5 mg/ml in PBS and administered at 25 µg/g mouse weigh via i.p. injection 3–4 h before embryo dissection. In ex vivo culture, EdU was added to cells at 10 µM 0–3 h after seeding.

Flow cytometry and qRT-PCR

Embryos were dissected at E9.5–11.5 in cold PBS and the posterior fragment or gonads dissociated in 0.25% trypsin/EDTA for 3 min at 37°C followed by 1 mg/ml Dnase I to dissolve any lingering clumps of tissue. Dead cells were excluded on the basis of Sytox Blue (Invitrogen) signal. PGCs were delineated as Oct4-ΔPE-GFP$^+$. Hindgut cells were live-stained for E-cadherin (1:200; #13–1900; Invitrogen) and sorted away from E-cad$^+$;GFP$^+$ PGCs. Gonadal soma was microdissected away from the mesonephros and depleted of GFP$^+$ PGCs. Each cell type was sorted directly into lysis buffer and extracted with the appropriate RNeasy kit (QIAGEN), DNase I treated, and reverse-transcribed with qScript (Quanta Biosciences) or Superscript III (Invitrogen). PCR primers were designed with Primer Express software (Applied Biosystems) or Primer-BLAST (NCBI). Amplification was performed with 50 or 100 cell equivalents of cDNA on a Mastercycler EP (Eppendorf) using the following primer sets for established Wnt target genes from the Wnt Homepage (http://web.stanford.edu/group/nusselab/cgi-bin/wnt): *Wnt5a*: 5′-CCAGTTCCGGCATCGGAGATGGA-3′, 5′-CACCGCGTACGTGAAGGCCG-3′; *Wnt3a*: 5′-GCACCACCGTCAGCAACAGCC-3′, 5′-AGCGGAGGCGATGGCATGGACA-3′; *Dkk1*: 5′-GCTTGCCGAAAGCGCAGGAAGC-3′, 5′-AGGAAAATGGCTGTGGTCAGAGGGC-3′; *Sfrp1*: 5′-ATGTGACAAGTTCCCCGAGGGCG-3′, 5′-TTGTCGCATGGAGGACACACGGT-3′; *Axin2*: 5′-TCGGGCCACCGCGAGTGTGA-3′, 5′-TGGCTGGTGCAAAGACATAGCCGGA-3′; *Ccnd1*: 5′-CTGAACCTGGGCAGCCCCAACA-3′, 5′-TTCCTGGCAGGCACGGAGGCA-3′; *Cdh1*: 5′-CCCTCATGAGCGTGCCCCAGT-3′, 5′-GGGTCGCTGTCGGCTGCCTT-3′; *Fn1*: 5′-CCCGCCACTGATTGGCCAGCAA-3′, 5′-GCGCACAGAGACGGCAGGGG-3′; *Lef1*: 5′-TCCGGGATCCCACCCGTCACAC-3′, 5′-TCCAACGCCGCCCGGAGACA-3′; *Dppa3*: 5′-AAAAAGGCTCGAAGGAAATGA-3′, 5′-AATTCTTCCCGATTTTCGCA-3′; *Gapdh*: 5′-GACTTCAACAGCAACTCCCAC-3′, 5′-AGGAAGGCTGGAAAAGAGCC-3′; *L7*: 5′-AGCGGATTGCCTTGACAGAT-3′, 5′-AACTTGAAGGGCCACAGGAA-3′.

PGC ex vivo culture

Oct4-ΔPE-GFP$^+$ PGCs sorted from E9.5 embryos were seeded in chambered slides (Lab-Tek II) coated with 1 mg/ml Matrigel (#354234; BD) then incubated at 37°C in 5% CO_2 with DMEM/15% Knockout Serum Replacement (Invitrogen), 1,000 U/ml LIF (EMD Millipore), 5 µM Forskolin (#F3917; Sigma-Aldrich), and 50 ng/ml SCF (#PMC2115; Invitrogen). WNT5a was added to media at 250 ng/ml (#645-WN/CF; R&D Systems). PGC numbers were counted at 3 h in culture and before time of fixation (18–24 h). After culture, cells were fixed for 10–15 min in 4% PFA and immunostained.

Somatic cells from E9.5 WT tails were digested using 0.25% trypsin/EDTA and cultured directly with endogenous PGCs. MEFs were generated from the posterior region of E13.5 WT and Wnt5a$^{-/-}$ embryos. Embryonic tissue was trypsinized for 30–45 min at 37° and triturated in DMEM/10% fetal calf serum. Cells were grown to confluency for 3–4 d, passaged to expand the population, and frozen in liquid nitrogen until use (Hogan et al., 1994). Conditioned media from E9.5 tail somatic cells was collected 16–20 h after dissociated posteriors were seeded in culture.

For BrdU experiments, hindguts and dorsal mesentery from E9.5 to 10.5 embryos were dissociated in 0.25% trypsin with 1 mg/ml DNase I at 37°C for 5 min. Digestion was stopped with FCS, and suspensions were seeded onto mitomycin C–treated STO fibroblast monolayers in chambered slides (Lab-Tek II), then incubated for 24 h at 37°C in 5% CO_2 with DMEM/10% FCS. After a 1-h treatment with 10 ng/ml BrdU, cells were fixed for 10 min in 4% PFA and immunostained.

Immunostaining

Embryos fixed in 4% PFA were embedded in OCT and cryosectioned at a thickness of 10 µm. Slides were blocked 1 h in 10% calf serum + 0.1% Triton X-100 in PBS and stained overnight at 4°C in the blocking

buffer followed by three 15-min washes in PBS. Primary antibodies used included *β-catenin* (rabbit, 1:25; #9582s; Cell Signaling Technology), *Axin2* (goat, Conductin M-20, 1:100; #sc-8570; Santa Cruz Biotechnology, Inc.), GFP (chicken, Aves GFP-1020, 1:200), SSEA1 (mouse IgM, 1:200; MC-480; Developmental Studies Hybridoma Bank), *Vasa* (rabbit, 1:400; #ab13840-100; Abcam), cleaved PARP (rabbit, 1:50; #9544s; Cell Signaling Technology), *E-cadherin* (rat, 1:200; #13–1900; Invitrogen), *Wnt5a* (goat, 1:20; #AF645; R&D Systems), and *Stella* (rabbit, 1:100; #ab19878; Abcam). Histological staining for *β-catenin* was preceded by 10 min additional fixation in 4% PFA and 3 min treatment in undiluted Ficin (Invitrogen) at room temperature followed by a quick PBS wash. This treatment was not necessary for *β-catenin* staining on cultured cells. EdU was labeled per kit protocol (#C10338 or C10340; Thermo Fisher Scientific). Secondary antibodies were purchased from Invitrogen and incubated for 1 h in blocking buffer at room temperature at 1:200. Nuclei were labeled with DAPI or Hoechst (1:1,000; Roche or Sigma-Aldrich). Sections were mounted in Vectashield (Vector Laboratories).

Image collection and analysis

Bright-field imaging was performed on an Olympus MVX10 stereomicroscope and Olympus acquisition software. Confocal imaging was performed at room temperature with a 20× 0.7 dry objective or 40× 0.95 oil-immersion objective on an SP5 TCS microscope (Leica) equipped with 405-, 488-, 543-, 594-, and 633-nm lasers. Use of the 20× objective typically required the addition of a 2× digital zoom for optimal visualization of PGCs for quantification. Files of 1,024 × 1,024 pixel images with 1- to 5-µm z-stacks were captured by a scanner with maximal frame resolution and acquisition software (Leica).

In vivo, mean nuclear *β-catenin* intensity was measured by comparing the signal within individual PGC nuclei to the mean signal of all nuclei in the image (>700). We devised a protocol in Volocity image processing software (PerkinElmer) to accurately obtain *β-catenin* signal intensity in each cell. PGCs were identified in the GFP or SSEA1 channel using the following series of commands: ‘‘Find Objects” using the software’s automatic threshold or manual SD intensity; “Fill Holes in Objects”; “Separate Touching Objects” using a size guide of ∼400 µm^3; and “Exclude Objects by Size” for objects smaller than ∼150 µm^3. Selected objects were visually inspected and changes were manually made to ensure appropriate selection of PGCs per image. Cell nuclei were identified in the DAPI/Hoechst channel using the same task commands described for PGCs, but with smaller size cutoffs. PGC nuclei were identified by overlapping PGC objects with nuclei objects via the “Intersect” command. All intensity measurements from PGC and total nuclei were exported to Excel (Microsoft) for calculations.

Ex vivo, mean nuclear *β-catenin, Axin2*, and *E-Cadherin* intensity in cultured PGCs was measured by comparing the signal within individual PGCs to the mean signal of all PGCs in the control well (ISO). We used the same identification protocol for the PGCs and nuclei as described for in vivo measurements to collect signal intensity in individual PGCs. Objects were visually inspected and changes were made manually to ensure appropriate selection of PGCs and nuclei; somatic cell nuclei were not collected. Measurements were exported to Excel for calculations.

To account for variability in staining between sections and between slides, we normalized nuclear *β-catenin* in vivo as follows: individual PGC n-βcat/mean n-βcat of image. Normalization in ex vivo cultured PGCs was calculated as follows: individual PGC n-βcat/mean n-βcat of control well (ISO).

Microarray analysis

Targeted gene expression of E9.5 PGCs was analyzed using a GeneChip Mouse Gene 1.0 ST Array (Affymetrix). Oct4-ΔPE-GFP$^+$ PGCs from single embryos were sorted into lysis buffer, extracted with RNeasy Micro kit (74004; QIAGEN), and sent to the University of California, San Francisco, Gladstone Genomics Core Facility for small sample amplification, microarray processing, and probe intensity normalization into a logarithm base 2 value. Intensity values for select Wnt target genes were normalized to housekeeping probe *Gapdh*. The raw data files can be downloaded from the Gene Expression Omnibus (GSE60179).

Bioinformatics

Microarray data were analyzed by AVC with dChip (Li and Wong, 2001) and Ingenuity Pathway Analysis (QIAGEN) to identify misregulated genes and associated functional categories. Additional analysis was performed by the Bioinformatics Core at the Gladstone Institutes, University of California, San Francisco. Microarrays were normalized for array-specific effects using Affymetrix’s “Robust Multi-Array” normalization. This was performed using the Affymetrix tool “apt-probeset-summarize,” which is part of the “Affymetrix Power Tools” package, available at http://www.affymetrix.com/estore/partners_programs/programs/developer/tools/powertools.affx. Normalized arrays values were reported on a log2 scale. (Mean normalized expression is typically ∼7.0.) For statistical analyses, we removed all array probesets where no experimental groups had a mean log2 intensity >3.0. This is a standard cutoff, below which expression is indistinguishable from background noise. Linear models were fitted for each gene using the Bioconductor “limma” package in R (Gentleman et al., 2004; Smyth, 2004). Moderated t-statistics, fold change, and the associated p-values were calculated for each gene. To account for the fact that thousands of genes were tested, we reported false discovery rate (FDR)–adjusted values, calculated using the Benjamini-Hochberg method (Benjamini and Hochberg, 1995). FDR values indicate the expected fraction of falsely declared differentially expressed (DE) genes among the total set of declared DE genes (i.e., FDR = 0.15 would indicate that ∼15% of the declared DE genes were expected to be caused by experimental noise instead of actual differential expression). Batch effects between the *Ror2^{Y324C}* and *β-catenin^{GOF}* microarray datasets were adjusted using “removeBatchEffect” in “limma” package in R. Comparisons were conducted on $n = 4$ WT and $n = 4$ *Ror2^{Y324C}* embryos for the *Ror2^{Y324C}* dataset and $n = 5$ WT and $n = 2$ *β-catenin^{GOF}* embryos for the *β-catenin^{GOF}* dataset.

GSEA of the *Ror2^{Y324C}* microarray dataset were compared with lists of cell cycle genes (Cell Cycle PCR Array; QIAGEN), *β-catenin* ChIP peaks called from mouse intestinal crypts (Schuijers et al., 2015), and misregulated genes identified in the *β-catenin^{GOF}* microarray dataset. Analyses were conducted using GSEA software downloaded from the Broad Institute at http://software.broadinstitute.org/gsea/index.jsp (Mootha et al., 2003; Subramanian et al., 2005). Files input comprised of *Ror2^{Y324C}* expression data (expression dataset, .txt file), gene lists of interest (gene sets database, .gmx file), labels for the expression data (phenotype labels, .cls file), and annotation of Affymetrix MoGene 1.0 ST microarray chips provided by the Broad Institute (Chip platform, .chip file). Details for the creation of each file type can be found in the GSEA user guide. Each analysis was performed as a *Ror2^{Y324C}* versus WT comparison and ran 1,000 permutations where the dataset was not collapsed to gene symbols (marked “false”), “phenotype” was selected as the permutation type, and minimum/maximum sizes were 20/5,000.

Statistics

Statistical tests including the Student’s *t* test, Fisher’s exact test, χ^2 test, correlation coefficient, regression analysis, and analysis of variance were performed in Excel (Microsoft), Prism (GraphPad), and VassarStats.

Online supplemental material

Fig. S1 shows examples of EdU labeling in embryo sections and frequency of EdU incorporation by location at specific ages and in different genetic backgrounds. Fig. S2 shows PGC distribution in *Ror2*^{Y324C} and *Wnt5a*$^{-/-}$ embryos by age, frequency of EdU incorporation by location at specific ages in each mutant, and localization of WNT5A in the hindgut. Fig. S3 shows rescue of BrdU incorporation in *Ror2*^{Y324C} mutants by *β-catenin* haploinsufficiency, overlap and GSEA enrichment of *Ror2*^{Y324C} misregulated genes with *β-catenin* ChIP in the mouse intestine, qRT-PCR of candidate Wnt modulators in several embryonic somatic location, and nuclear *β-catenin* levels in *Ror2*^{Y324C} PGCs treated with exogenous WNT5a. Fig. S4 shows the effect of Ficin treatment on revealing nuclear *β-catenin* signal in histological sections and quantification of nuclear *β-catenin* intensity in PGCs in all migratory ages and in specific locations by age. Fig. S5 shows *Pou5f1*$^{cre\text{-}ER}$ activity with tamoxifen exposure at E8.25 and PGC distribution and EdU incorporation across embryonic locations in *β-catenin*^{GOF} mutants. Online supplemental material is available at http://www.jcb.org/cgi/content/full/jcb.201511061/DC1.

Acknowledgments

The authors thank A. Brack, R. Arora, D. Nguyen, B. Reznik, N. Meyer, B. DeVeale, and K. Ebata for feedback on versions of this manuscript; M. Kissner and A.D.J. Ross for technical support; J. Schuijers and H. Clevers for sharing *β-catenin* ChIP annotations and data; A. Williams at the Gladstone Bioinformatics Core for statistical analysis of microarray data; and A. Laird for guidance on statistics.

This work was supported by a National Science Foundation predoctoral fellowship to A.V. Cantú, the University of California, San Francisco Program for Breakthrough Biomedical Research, and National Institutes of Health grants 1R21ES023297-01 and DP2OD007420 to D.J. Laird.

The authors declare no competing financial interests.

Author contributions: A.V. Cantú, S. Altshuler-Keylin, and D.J. Laird designed the study; A.V. Cantú and D.J. Laird wrote the manuscript; and all authors carried out experiments and contributed to data analysis.

Submitted: 16 November 2015
Accepted: 15 June 2016

References

Anderson, R., R. Fässler, E. Georges-Labouesse, R.O. Hynes, B.L. Bader, J.A. Kreidberg, K. Schaible, J. Heasman, and C. Wylie. 1999. Mouse primordial germ cells lacking β1 integrins enter the germline but fail to migrate normally to the gonads. *Development.* 126:1655–1664.

Ara, T., Y. Nakamura, T. Egawa, T. Sugiyama, K. Abe, T. Kishimoto, Y. Matsui, and T. Nagasawa. 2003. Impaired colonization of the gonads by primordial germ cells in mice lacking a chemokine, stromal cell-derived factor-1 (SDF-1). *Proc. Natl. Acad. Sci. USA.* 100:5319–5323. http://dx.doi.org/10.1073/pnas.0730719100

Aramaki, S., K. Hayashi, K. Kurimoto, H. Ohta, Y. Yabuta, H. Iwanari, Y. Mochizuki, T. Hamakubo, Y. Kato, K. Shirahige, and M. Saitou. 2013. A mesodermal factor, T, specifies mouse germ cell fate by directly activating germline determinants. *Dev. Cell.* 27:516–529. http://dx.doi.org/10.1016/j.devcel.2013.11.001

Arora, R., E. Altman, N.D. Tran, and D.J. Laird. 2014. Novel domains of expression for orphan receptor tyrosine kinase Ror2 in the human and mouse reproductive system. *Dev. Dyn.* 243:1037–1045. http://dx.doi.org/10.1002/dvdy.24138

Behrens, J., J.P. von Kries, M. Kühl, L. Bruhn, D. Wedlich, R. Grosschedl, and W. Birchmeier. 1996. Functional interaction of beta-catenin with the transcription factor LEF-1. *Nature.* 382:638–642. http://dx.doi.org/10.1038/382638a0

Bendel-Stenzel, M.R., M. Gomperts, R. Anderson, J. Heasman, and C. Wylie. 2000. The role of cadherins during primordial germ cell migration and early gonad formation in the mouse. *Mech. Dev.* 91:143–152. http://dx.doi.org/10.1016/S0925-4773(99)00287-7

Benjamini, Y., and Y. Hochberg. 1995. Controlling the false discovery rate: a practical and powerful approach to multiple testing. *J. R. Stat. Soc. B.* 57:289–300.

Bialecka, M., T. Young, S. Chuva de Sousa Lopes, D. ten Berge, A. Sanders, F. Beck, and J. Deschamps. 2012. Cdx2 contributes to the expansion of the early primordial germ cell population in the mouse. *Dev. Biol.* 371:227–234. http://dx.doi.org/10.1016/j.ydbio.2012.08.018

Brault, V., R. Moore, S. Kutsch, M. Ishibashi, D.H. Rowitch, A.P. McMahon, L. Sommer, O. Boussadia, and R. Kemler. 2001. Inactivation of the β-catenin gene by Wnt1-Cre-mediated deletion results in dramatic brain malformation and failure of craniofacial development. *Development.* 128:1253–1264.

Burt, A., and R. Trivers. 2006. Genes in Conflict: The Biology of Selfish Genetic Elements. Belknap Press of Harvard University Press, Cambridge, MA. http://dx.doi.org/10.4159/9780674029118

Cervantes, S., T.P. Yamaguchi, and M. Hebrok. 2009. Wnt5a is essential for intestinal elongation in mice. *Dev. Biol.* 326:285–294. http://dx.doi.org/10.1016/j.ydbio.2008.11.020

Chassot, A.A., F. Ranc, E.P. Gregoire, H.L. Roepers-Gajadien, M.M. Taketo, G. Camerino, D.G. de Rooij, A. Schedl, and M.C. Chaboissier. 2008. Activation of β-catenin signaling by Rspo1 controls differentiation of the mammalian ovary. *Hum. Mol. Genet.* 17:1264–1277. http://dx.doi.org/10.1093/hmg/ddn016

Chassot, A.A., E.P. Gregoire, R. Lavery, M.M. Taketo, D.G. de Rooij, I.R. Adams, and M.C. Chaboissier. 2011. RSPO1/β-catenin signaling pathway regulates oogonia differentiation and entry into meiosis in the mouse fetal ovary. *PLoS One.* 6:e25641. http://dx.doi.org/10.1371/journal.pone.0025641

Chassot, A.A., S.T. Bradford, A. Auguste, E.P. Gregoire, E. Pailhoux, D.G. de Rooij, A. Schedl, and M.C. Chaboissier. 2012. WNT4 and RSPO1 together are required for cell proliferation in the early mouse gonad. *Development.* 139:4461–4472. http://dx.doi.org/10.1242/dev.078972

Chawengsaksophak, K., T. Svingen, E.T. Ng, T. Epp, C.M. Spiller, C. Clark, H. Cooper, and P. Koopman. 2012. Loss of Wnt5a disrupts primordial germ cell migration and male sexual development in mice. *Biol. Reprod.* 86:1–12. http://dx.doi.org/10.1095/biolreprod.111.095232

Chiquoine, A.D. 1954. The identification, origin, and migration of the primordial germ cells in the mouse embryo. *Anat. Rec.* 118:135–146. http://dx.doi.org/10.1002/ar.1091180202

de Vries, W.N., L.T. Binns, K.S. Fancher, J. Dean, R. Moore, R. Kemler, and B.B. Knowles. 2000. Expression of Cre recombinase in mouse oocytes: a means to study maternal effect genes. *Genesis.* 26:110–112. http://dx.doi.org/10.1002/(SICI)1526-968X(200002)26:2<110::AID-GENE2>3.0.CO;2-8

Downs, K.M. 2008. Systematic localization of Oct-3/4 to the gastrulating mouse conceptus suggests manifold roles in mammalian development. *Dev. Dyn.* 237:464–475. http://dx.doi.org/10.1002/dvdy.21438

Edris, B., I. Espinosa, T. Mühlenberg, A. Mikels, C.H. Lee, S.E. Steigen, S. Zhu, K.D. Montgomery, A.J. Lazar, D. Lev, et al. 2012. ROR2 is a novel prognostic biomarker and a potential therapeutic target in leiomyosarcoma and gastrointestinal stromal tumour. *J. Pathol.* 227:223–233. http://dx.doi.org/10.1002/path.3986

Gentleman, R.C., V.J. Carey, D.M. Bates, B. Bolstad, M. Dettling, S. Dudoit, B. Ellis, L. Gautier, Y. Ge, J. Gentry, et al. 2004. Bioconductor: open software development for computational biology and bioinformatics. *Genome Biol.* 5:R80. http://dx.doi.org/10.1186/gb-2004-5-10-r80

Gomperts, M., M. Garcia-Castro, C. Wylie, and J. Heasman. 1994. Interactions between primordial germ cells play a role in their migration in mouse embryos. *Development.* 120:135–141.

Greder, L.V., S. Gupta, S. Li, M.J. Abedin, A. Sajini, Y. Segal, J.M.W. Slack, and J.R. Dutton. 2012. Analysis of endogenous Oct4 activation during induced pluripotent stem cell reprogramming using an inducible Oct4 lineage label. *Stem Cells.* 30:2596–2601. http://dx.doi.org/10.1002/stem.1216

Gu, Y., C. Runyan, A. Shoemaker, A. Surani, and C. Wylie. 2009. Steel factor controls primordial germ cell survival and motility from the time of their specification in the allantois, and provides a continuous niche throughout their migration. *Development.* 136:1295–1303. http://dx.doi.org/10.1242/dev.030619

Haegel, H., L. Larue, M. Ohsugi, L. Fedorov, K. Herrenknecht, and R. Kemler. 1995. Lack of β-catenin affects mouse development at gastrulation. *Development.* 121:3529–3537.

Harada, N., Y. Tamai, T. Ishikawa, B. Sauer, K. Takaku, M. Oshima, and M.M. Taketo. 1999. Intestinal polyposis in mice with a dominant stable mutation of the β-catenin gene. *EMBO J.* 18:5931–5942. http://dx.doi.org/10.1093/emboj/18.21.5931

Hikasa, H., M. Shibata, I. Hiratani, and M. Taira. 2002. The *Xenopus* receptor tyrosine kinase Xror2 modulates morphogenetic movements of the axial mesoderm and neuroectoderm via Wnt signaling. *Development.* 129:5227–5239.

Ho, H.Y., M.W. Susman, J.B. Bikoff, Y.K. Ryu, A.M. Jonas, L. Hu, R. Kuruvilla, and M.E. Greenberg. 2012. Wnt5a-Ror-Dishevelled signaling constitutes a core developmental pathway that controls tissue morphogenesis. *Proc. Natl. Acad. Sci. USA.* 109:4044–4051. http://dx.doi.org/10.1073/pnas.1200421109

Hogan, B., R. Beddington, F. Constantini, and E. Lacy. 1994. Manipulating the Mouse Embryo. 3rd. Cold Spring Harbor Laboratory Press, Cold Spring Harbor, NY. 800 pp.

Huelsken, J., R. Vogel, V. Brinkmann, B. Erdmann, C. Birchmeier, and W. Birchmeier. 2000. Requirement for β-catenin in anterior-posterior axis formation in mice. *J. Cell Biol.* 148:567–578. http://dx.doi.org/10.1083/jcb.148.3.567

Jamora, C., R. DasGupta, P. Kocieniewski, and E. Fuchs. 2003. Links between signal transduction, transcription and adhesion in epithelial bud development. *Nature.* 422:317–322. http://dx.doi.org/10.1038/nature01458

Jho, E.H., T. Zhang, C. Domon, C.K. Joo, J.N. Freund, and F. Costantini. 2002. Wnt/beta-catenin/Tcf signaling induces the transcription of Axin2, a negative regulator of the signaling pathway. *Mol. Cell. Biol.* 22:1172–1183. http://dx.doi.org/10.1128/MCB.22.4.1172-1183.2002

Kaufman, M.H. 1992. The Atlas of Mouse Development. Elsevier Academic Press, London. 512 pp.

Kispert, A., S. Vainio, L. Shen, D.H. Rowitch, and A.P. McMahon. 1996. Proteoglycans are required for maintenance of Wnt-11 expression in the ureter tips. *Development.* 122:3627–3637.

Kunwar, P.S., D.E. Siekhaus, and R. Lehmann. 2006. In vivo migration: a germ cell perspective. *Annu. Rev. Cell Dev. Biol.* 22:237–265. http://dx.doi.org/10.1146/annurev.cellbio.22.010305.103337

Laird, D.J., U.H. von Andrian, and A.J. Wagers. 2008. Stem cell trafficking in tissue development, growth, and disease. *Cell.* 132:612–630. http://dx.doi.org/10.1016/j.cell.2008.01.041

Laird, D.J., S. Altshuler-Keylin, M.D. Kissner, X. Zhou, and K.V. Anderson. 2011. Ror2 enhances polarity and directional migration of primordial germ cells. *PLoS Genet.* 7:e1002428. http://dx.doi.org/10.1371/journal.pgen.1002428

Li, C., and W.H. Wong. 2001. Model-based analysis of oligonucleotide arrays: expression index computation and outlier detection. *Proc. Natl. Acad. Sci. USA.* 98:31–36. http://dx.doi.org/10.1073/pnas.98.1.31

Logan, C.Y., and R. Nusse. 2004. The Wnt signaling pathway in development and disease. *Annu. Rev. Cell Dev. Biol.* 20:781–810. http://dx.doi.org/10.1146/annurev.cellbio.20.010403.113126

Lu, B.J., Y.Q. Wang, X.J. Wei, L.Q. Rong, D. Wei, C.M. Yan, D.J. Wang, and J.Y. Sun. 2012. Expression of WNT-5a and ROR2 correlates with disease severity in osteosarcoma. *Mol. Med. Rep.* 5:1033–1036. http://dx.doi.org/10.3892/MMR.2012.772

Lustig, B., B. Jerchow, M. Sachs, S. Weiler, T. Pietsch, U. Karsten, M. van de Wetering, H. Clevers, P.M. Schlag, W. Birchmeier, and J. Behrens. 2002. Negative feedback loop of Wnt signaling through upregulation of conductin/axin2 in colorectal and liver tumors. *Mol. Cell. Biol.* 22:1184–1193. http://dx.doi.org/10.1128/MCB.22.4.1184-1193.2002

Matsui, Y., K. Zsebo, and B.L.M. Hogan. 1992. Derivation of pluripotential embryonic stem cells from murine primordial germ cells in culture. *Cell.* 70:841–847. http://dx.doi.org/10.1016/0092-8674(92)90317-6

McLaren, A. 2003. Primordial germ cells in the mouse. *Dev. Biol.* 262:1–15. http://dx.doi.org/10.1016/S0012-1606(03)00214-8

Mikels, A.J., and R. Nusse. 2006. Purified Wnt5a protein activates or inhibits β-catenin-TCF signaling depending on receptor context. *PLoS Biol.* 4:e115. http://dx.doi.org/10.1371/journal.pbio.0040115

Mikels, A., Y. Minami, and R. Nusse. 2009. Ror2 receptor requires tyrosine kinase activity to mediate Wnt5A signaling. *J. Biol. Chem.* 284:30167–30176. http://dx.doi.org/10.1074/jbc.M109.041715

Molyneaux, K.A., H. Zinszner, P.S. Kunwar, K. Schaible, J. Stebler, M.J. Sunshine, W. O'Brien, E. Raz, D. Littman, C. Wylie, and R. Lehmann. 2003. The chemokine SDF1/CXCL12 and its receptor CXCR4 regulate mouse germ cell migration and survival. *Development.* 130:4279–4286. http://dx.doi.org/10.1242/dev.00640

Moon, R.T., R.M. Campbell, J.L. Christian, L.L. McGrew, J. Shih, and S. Fraser. 1993. Xwnt-5A: a maternal Wnt that affects morphogenetic movements after overexpression in embryos of *Xenopus laevis*. *Development.* 119:97–111.

Mootha, V.K., C.M. Lindgren, K.F. Eriksson, A. Subramanian, S. Sihag, J. Lehar, P. Puigserver, E. Carlsson, M. Ridderstråle, E. Laurila, et al. 2003. PGC-1α-responsive genes involved in oxidative phosphorylation are coordinately downregulated in human diabetes. *Nat. Genet.* 34:267–273. http://dx.doi.org/10.1038/ng1180

Muzumdar, M.D., B. Tasic, K. Miyamichi, L. Li, and L. Luo. 2007. A global double-fluorescent Cre reporter mouse. *Genesis.* 45:593–605. http://dx.doi.org/10.1002/dvg.20335

Niehrs, C. 2012. The complex world of WNT receptor signalling. *Nat. Rev. Mol. Cell Biol.* 13:767–779. http://dx.doi.org/10.1038/nrm3470

Nieuwkoop, P.D., and L.A. Satasurya. 1979. Primordial Germ Cells in the Chordates: Embryogenesis and Phylogenesis. Cambridge University Press, Cambridge, UK. 192 pp.

Nieuwkoop, P.D., and L.A. Satasurya. 1981. Primordial Germ Cells in the Invertebrates. Cambridge University Press, Cambridge, UK. 272 pp.

Ohinata, Y., H. Ohta, M. Shigeta, K. Yamanaka, T. Wakayama, and M. Saitou. 2009. A signaling principle for the specification of the germ cell lineage in mice. *Cell.* 137:571–584. http://dx.doi.org/10.1016/j.cell.2009.03.014

Oishi, I., H. Suzuki, N. Onishi, R. Takada, S. Kani, B. Ohkawara, I. Koshida, K. Suzuki, G. Yamada, G.C. Schwabe, et al. 2003. The receptor tyrosine kinase Ror2 is involved in non-canonical Wnt5a/JNK signalling pathway. *Genes Cells.* 8:645–654. http://dx.doi.org/10.1046/j.1365-2443.2003.00662.x

Resnick, J.L., L.S. Bixler, L. Cheng, and P.J. Donovan. 1992. Long-term proliferation of mouse primordial germ cells in culture. *Nature.* 359:550–551. http://dx.doi.org/10.1038/359550a0

Richardson, B.E., and R. Lehmann. 2010. Mechanisms guiding primordial germ cell migration: strategies from different organisms. *Nat. Rev. Mol. Cell Biol.* 11:37–49. http://dx.doi.org/10.1038/nrm2815

Runyan, C., K. Schaible, K. Molyneaux, Z. Wang, L. Levin, and C. Wylie. 2006. Steel factor controls midline cell death of primordial germ cells and is essential for their normal proliferation and migration. *Development.* 133:4861–4869. http://dx.doi.org/10.1242/dev.02688

Sato, A., H. Yamamoto, H. Sakane, H. Koyama, and A. Kikuchi. 2010. Wnt5a regulates distinct signalling pathways by binding to Frizzled2. *EMBO J.* 29:41–54. http://dx.doi.org/10.1038/emboj.2009.322

Schuijers, J., J.P. Junker, M. Mokry, P. Hatzis, B.K. Koo, V. Sasselli, L.G. van der Flier, E. Cuppen, A. van Oudenaarden, and H. Clevers. 2015. Ascl2 acts as an R-spondin/Wnt-responsive switch to control stemness in intestinal crypts. *Cell Stem Cell.* 16:158–170. http://dx.doi.org/10.1016/j.stem.2014.12.006

Seki, Y., M. Yamaji, Y. Yabuta, M. Sano, M. Shigeta, Y. Matsui, Y. Saga, M. Tachibana, Y. Shinkai, and M. Saitou. 2007. Cellular dynamics associated with the genome-wide epigenetic reprogramming in migrating primordial germ cells in mice. *Development.* 134:2627–2638. http://dx.doi.org/10.1242/dev.005611

Smyth, G.K. 2004. Linear models and empirical Bayes methods for assessing differential expression in microarray experiments. *Stat. Appl. Genet. Mol. Biol.* 3:Article3.

Subramanian, A., P. Tamayo, V.K. Mootha, S. Mukherjee, B.L. Ebert, M.A. Gillette, A. Paulovich, S.L. Pomeroy, T.R. Golub, E.S. Lander, and J.P. Mesirov. 2005. Gene set enrichment analysis: a knowledge-based approach for interpreting genome-wide expression profiles. *Proc. Natl. Acad. Sci. USA.* 102:15545–15550. http://dx.doi.org/10.1073/pnas.0506580102

Takada, S., K.L. Stark, M.J. Shea, G. Vassileva, J.A. McMahon, and A.P. McMahon. 1994. Wnt-3a regulates somite and tailbud formation in the mouse embryo. *Genes Dev.* 8:174–189. http://dx.doi.org/10.1101/gad.8.2.174

Tam, P.P.L., and M.H.L. Snow. 1981. Proliferation and migration of primordial germ cells during compensatory growth in mouse embryos. *J. Embryol. Exp. Morphol.* 64:133–147.

Tanaka, S.S., A. Nakane, Y.L. Yamaguchi, T. Terabayashi, T. Abe, K. Nakao, M. Asashima, K.A. Steiner, P.P. Tam, and R. Nishinakamura. 2013. Dullard/Ctdnep1 modulates WNT signalling activity for the formation of primordial germ cells in the mouse embryo. *PLoS One.* 8:e57428. http://dx.doi.org/10.1371/journal.pone.0057428

Vainio, S., M. Heikkilä, A. Kispert, N. Chin, and A.P. McMahon. 1999. Female development in mammals is regulated by Wnt-4 signalling. *Nature.* 397:405–409. http://dx.doi.org/10.1038/17068

van Amerongen, R., and R. Nusse. 2009. Towards an integrated view of Wnt signaling in development. *Development.* 136:3205–3214. http://dx.doi.org/10.1242/dev.033910

van Amerongen, R., C. Fuerer, M. Mizutani, and R. Nusse. 2012. Wnt5a can both activate and repress Wnt/β-catenin signaling during mouse embryonic

development. *Dev. Biol.* 369:101–114. http://dx.doi.org/10.1016/j.ydbio.2012.06.020

Weeraratna, A.T., Y. Jiang, G. Hostetter, K. Rosenblatt, P. Duray, M. Bittner, and J.M. Trent. 2002. Wnt5a signaling directly affects cell motility and invasion of metastatic melanoma. *Cancer Cell.* 1:279–288. http://dx.doi.org/10.1016/S1535-6108(02)00045-4

Wong, G.T., B.J. Gavin, and A.P. McMahon. 1994. Differential transformation of mammary epithelial cells by Wnt genes. *Mol. Cell. Biol.* 14:6278–6286. http://dx.doi.org/10.1128/MCB.14.9.6278

Yamada, M., J. Udagawa, A. Matsumoto, R. Hashimoto, T. Hatta, M. Nishita, Y. Minami, and H. Otani. 2010. Ror2 is required for midgut elongation during mouse development. *Dev. Dyn.* 239:941–953. http://dx.doi.org/10.1002/dvdy.22212

Yamaguchi, T.P., A. Bradley, A.P. McMahon, and S. Jones. 1999. A Wnt5a pathway underlies outgrowth of multiple structures in the vertebrate embryo. *Development.* 126:1211–1223.

Yamamoto, S., O. Nishimura, K. Misaki, M. Nishita, Y. Minami, S. Yonemura, H. Tarui, and H. Sasaki. 2008. Cthrc1 selectively activates the planar cell polarity pathway of Wnt signaling by stabilizing the Wnt-receptor complex. *Dev. Cell.* 15:23–36. http://dx.doi.org/10.1016/j.devcel.2008.05.007

Yan, D., M. Wiesmann, M. Rohan, V. Chan, A.B. Jefferson, L. Guo, D. Sakamoto, R.H. Caothien, J.H. Fuller, C. Reinhard, et al. 2001. Elevated expression of axin2 and hnkd mRNA provides evidence that Wnt/β-catenin signaling is activated in human colon tumors. *Proc. Natl. Acad. Sci. USA.* 98:14973–14978. http://dx.doi.org/10.1073/pnas.261574498